CHAPTER NINE

The Minerals and Structural Components of Iron Meteorites

The major minerals of the irons were recognized quite early. Thus when Rose (1864a) classified and described the Berlin meteorite collection, he was able to discuss the following minerals in some detail: kamacite, taenite, graphite, schreibersite, rhabdite (named by him), chromite, troilite and olivine. In Table 32 all the minerals presently described from iron meteorites and their silicate inclusions are listed. For further information the reader is referred to Cohen (1894; 1905), Perry (1944), Krinov (1960a), Mason (1962a; 1967a), Ramdohr (1966), Wood (1967) and Keil (1969). In these papers numerous other meteoritic minerals so far only identified in stone meteorites are also treated. A total of about 60 meteoritic minerals are known out of which about 20 are not known as terrestrial minerals. Furthermore, two dozen secondary minerals produced by terrestrial weathering of the meteorites are known (White et al. 1967; Mason 1967a; Yudin 1970). Only a few, such as goethite, α-FeOOH; maghemite, γ-Fe_2O_3; and pentlandite, $(Fe,Ni)_9S_8$, occur abundantly, the others are usually only present as traces or as the result of special circumstances. In the present work all terrestrial iron oxides are covered under the general terms "rust" or "limonite," because no further attempt was made to identify the corrosion products. Figures 93-95 show some typical corrosive effects on iron meteorites.

Comments on the primary major minerals and on a few accessories follow.

Kamacite. Ferritic iron with up to 7.5% Ni in solid solution is, when it occurs as a meteoritic mineral, called kamacite.

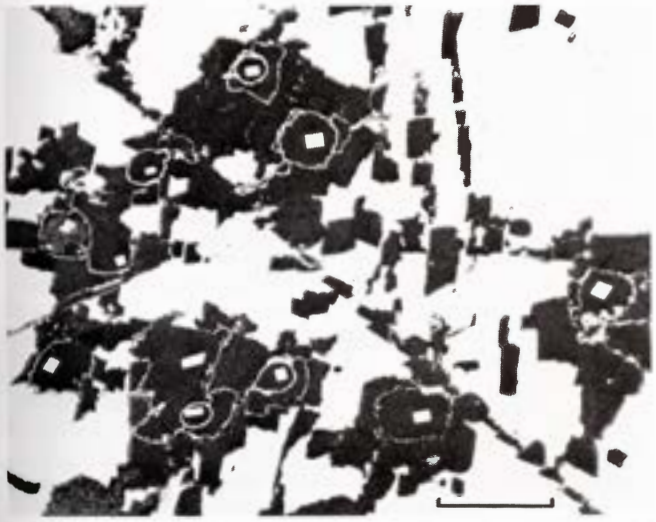

Figure 93. Corroded kamacite phase with rhabdite inclusions (white squares). Typical near-surface attack on hexahedrites and coarse octahedrites. Weathering has selectively attacked the nickel- and phosphorus-depleted ferrite adjacent to the phosphides. Polished. Scale bar 50 μ.

Figure 94. Corroded kamacite phase adjacent to taenite. The kamacite spindles of the plessite interior are also selectively converted to "limonite." Typical near-surface attack on octahedrites. Polished. Scale bar 50 μ.

The word comes from Greek *kamas* – i.e., bar, – and was proposed by Reichenbach (1861) to cover one of the three components in the "Trias," kamacite, taenite and plessite. The ferritic phase was thus recognized in iron meteorites before ferrite was identified as a component of steel.

The nickel is in solid solution in the kamacite, substituting for iron atoms in the body centered cubic lattice. Kamacite of hexahedrites contains 5.0-5.5% Ni, but anomalous hexahedrites may contain somewhat less, e.g., 4% in Tombigbee River. Kamacite of octahedrites contains 5.5-7.5% Ni, with a systematic variation of nickel with bandwidth (Figures 95A, 189A, 189B). Phosphorus atoms occur substitutionally for iron and nickel atoms in kamacite, usually up to about 0.06 weight % P. The distribution of Ni and P within individual kamacite lamellae has been thoroughly examined by Yavnel (1962), Massalski & Park (1962), Agrell et al. (1963), Wood (1964; 1967), Short & Andersen (1965), Goldstein (1965) and Reed (1967a, b; 1969). It has been found that the normal slowly cooled kamacite bands in octahedrites display a narrow Agrell depletion in Ni (a 1% dip) at the kamacite-taenite interface, and a broad (0.5%) dip in Ni content at the center of the bands.

In special circumstances the kamacite may be more depleted in nickel. When cohenite, with 1.5% Ni and 6.7% C, decomposes on cosmic annealing, the resultant structure displays kamacite with only 1.5% Ni and inter-

Table 32. Minerals of Unweathered Iron Meteorites

Name	Formula	Structure	References and notes
Kamacite[1]	α - Fe(Ni), Ni < 7.5%	body-centered cubic	Reichenbach 1861
Taenite[2]	γ - Fe(Ni), Ni > 25%	face-centered cubic	Reichenbach 1861
Graphite	C	hexagonal	Troost 1840; Haidinger 1846
Diamond	C	cubic	Foote 1891. See also page 384.
*Lonsdaleite	C	hexagonal	Frondel & Marvin 1967
Copper	Cu	f.c.c.	Nininger 1941; Ramdohr 1963a
Cohenite[1]	$(Fe,Ni)_3C$	rhombic	Weinschenk 1889. See also page 793.
*Haxonite	$(Fe,Ni)_{23}C_6$	cubic	Scott 1971
*Carlsbergite	CrN	cubic	Buchwald & Scott 1971
*Schreibersite, rhabdite	$(Fe,Ni)_3P$	tetragonal	Haidinger 1847; Rose 1864a:48. See also pages 793 and 1095.
Troilite[3]	FeS	hexagonal	Haidinger 1863a
Mackinawite	FeS	tetragonal	Ramdohr 1963a; El Goresy 1965
Sphalerite	ZnS	cubic	Ramdohr 1963a
*Brezinaite	Cr_3S_4	monoclinic	Bunch & Fuchs 1969
*Daubreelite	$FeCr_2S_4$	cubic	Smith 1876c, 1878
*Djerfisherite	$K_3CuFe_{12}S_{14}$	cubic	Fuchs 1966
oChalcopyrite	$CuFeS_2$	tetragonal	Ramdohr 1963
oPentlandite	$(Fe,Ni)_9S_8$	cubic	Sztrokay 1960; Fredriksson & Keil 1964
*Perryite	Ni_5Si_2 ?	hexagonal ?	Fredriksson & Henderson 1965; Keil 1968; and this work: page 661.
Chalcopyrrhotite	$CuFe_2S_3$	orthorhombic	Ramdohr 1963a
Ferromagnesian alabandite	$(Fe_{0.2}Mg_{0.3}Mn_{0.5})S$	cubic	Keil & Frederiksson 1963; El Goresy 1965
Cristobalite	SiO_2	tetragonal $\underset{\rightleftharpoons}{270}$° C cubic	Marvin 1962; Strunz 1970
Tridymite	SiO_2	monoclinic $\underset{\rightleftharpoons}{400}$° C hexagonal	Marvin 1962; Götz 1962; Dollase 1967
Rutile	TiO_2	tetragonal	Buseck & Keil 1966; El Goresy 1971
Ilmenite	$FeTiO_3$	hexagonal	Buseck & Keil 1966
Magnetite	Fe_3O_4	cubic	In iron meteorites only in the fusion crust. Kolomenskij & Yudin 1958; Marvin 1963. Magnetite in carbonaceous chondrites: Jedwab 1967; 1971
Wüstite	$Fe_{1-x}O$	cubic	
Chromite	$FeCr_2O_4$	cubic	Rose 1864a: 39; Cohen 1894: 244; Derby 1896
Merrilite = whitlockite	$Ca_3(PO_4)_2$	hexagonal	Fuchs 1962
Graftonite	$(Fe,Mn)_3(PO_4)_2$	monoclinic	Olsen & Fredriksson 1966
Sarcopside	$(Fe,Mn)_3(PO_4)_2$	monoclinic	Olsen & Fredriksson 1966
*Panethite	$Na_2Mg_2(PO_4)_2$	monoclinic	Fuchs et al. 1967
*Brianite	$Na_2MgCa(PO_4)_2$	monoclinic	Fuchs et al. 1967
*Farringtonite	$(Mg,Fe)_3(PO_4)_2$	monoclinic	Bild 1973 (personal communication).
Chlorapatite	$Ca_5(PO_4)_3Cl$	hexagonal	Fuchs & Olsen 1965; Marshall & Keil 1965
Zircon	$ZrSiO_4$	tetragonal	Laspeyres 1895; Marvin & Klein 1964
*Kosmochlor = ureyite	$NaCrSi_2O_6$	monoclinic	Laspeyres 1897; Frondel & Klein 1965; Neuhaus 1967
*Krinovite	$NaMg_2CrSi_3O_{10}$	monoclinic	Olsen & Fuchs 1968
*Yagiite	$(Na,K)_{1.5}Mg_2(Al,Mg,Fe)_3(Al_2Si_{10}O_{30})$	hexagonal	Bunch & Fuchs 1969
Richterite, an amphibole	$Na_2Ca(Mg,Fe)_5Si_8O_{22}(OH,F)_2$	monoclinic	Olsen 1967; Olsen et al. 1973
Olivine x = 0 forsterite; x = 1 fayalite	$(Mg_{1-x}Fe_x)SiO_4$	orthorhombic isomorphous group	Stromeyer 1824; Rose 1864a; Cohen 1894: 249; Keil & Fredriksson 1964
Orthopyroxenes[4] x < 0.12 enstatite; 0.12 < x < 0.3 bronzite; x > 0.3 hypersthene	$(Mg_{1-x}Fe_x)SiO_3$	orthorhombic isomorphous group	Derby 1896; Cohen 1894: 268; Marshall & Keil 1965; Mason 1968; Bunch et al. 1970
Clinopyroxenes, including augite, pigeonite, diopside etc.	$(Ca,Mg,Fe)SiO_3$	monoclinic isomorphous group	Same as for orthopyroxenes
Plagioclase feldspars, albite anorthite	$NaAlSi_3O_8$ $CaAl_2Si_2O_8$	triclinic isomorphous group	Cohen 1894: 301; Laspeyres 1895; Mason 1965; Bunch et al. 1970. Maskelynite is shock-produced plagioclase glass.

1) Kamacite and cohenite are extremely rare as terrestrial minerals, having been reported from Ovifak, Greenland (Löfquist & Benedicks 1941), from Bühl, Germany, and a few other places (Gmelin 1929: 141). They are deficient in nickel compared to the meteoritic occurrences.

2) Taenite with 25-50% Ni is apparently unknown as a terrestrial mineral. Awaruite Ni_3Fe, however, is well known (Nickel 1959).

3) Terrestrial pyrrhotites, $Fe_{1-x}S$, with stoichiometric composition have been reported, though these are rare (Deer et al. 1967: 145).

4) Deer et al. 1967.

* Not known to occur in terrestrial rocks.

o Probably in iron meteorites mainly (only ?) as secondary minerals from terrestrial weathering.

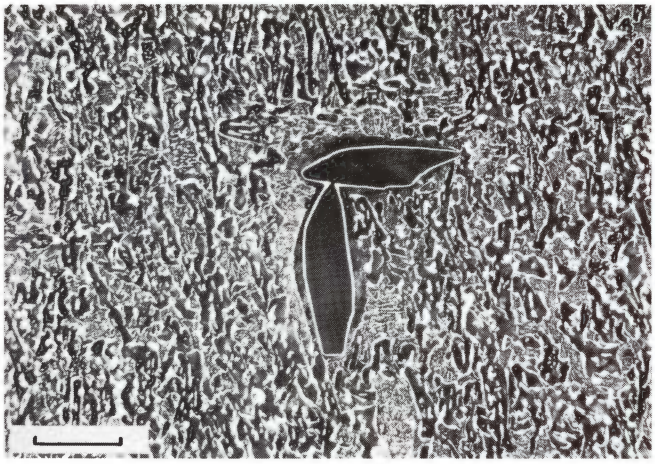

Figure 95. Tlacotepec (Copenhagen no. 1968, 338). Corroded kamacite phase. In near-surface areas of ataxites the scattered α-spindles and the fine-grained kamacite of the duplex plessite matrix are selectively corroded. Polished. Scale bar 20 μ.

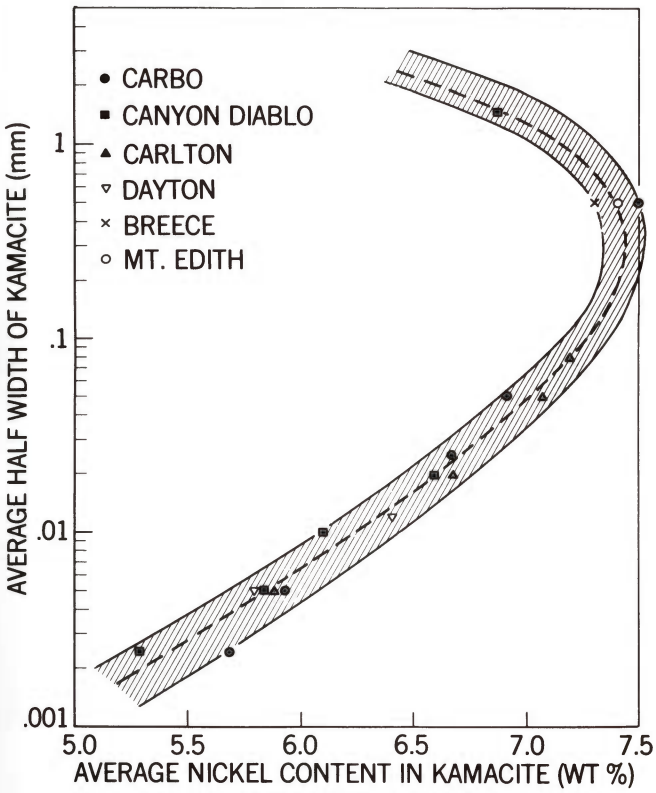

Figure 95A. Average Ni concentration in kamacite versus the average halfwidth of kamacite for several meteorites. (The Breece sample is a portion of the Grant meteorite). (From Goldstein 1967.)

calated 10 μ wide graphite lamellae. See, e.g., Wichita County, Oscuro Mountains and Dungannon. This indicates that the annealing took place at relatively low temperatures (< 500° C) so that Ni was not able to diffuse and equilibrate with the adjacent normal 5-7% Ni-kamacite.

Swathing kamacite is the name given to the rimming kamacite that envelops large troilite, schreibersite, and silicate inclusions to varying extents. It is obvious as 0.5-1.5 mm wide rims around troilite and schreibersite in group IIIA but in fact occurs in all classes and in widths down to a few microns.

Older theories about the formation of swathing kamacite involved the rejection of nickel-iron from supersaturated troilite and schreibersite (Perry 1944: 87; Henderson & Perry 1958: 379) or a complicated formation governed by intricate Fe-Ni-P diagram considerations (Vogel 1964). There is, however, little doubt that swathing kamacite is simply the first kamacite to form from taenite during the primary cooling. The solid state transformation usually starts around foreign inclusions, such as silicates, chromite, troilite and schreibersite, that act as heterogeneous nuclei. Later, when the temperature has dropped perhaps 50-100° C, and the kamacite rims have attained some size – depending upon nickel content and cooling rate, – the bulk of the taenite will transform homogene-

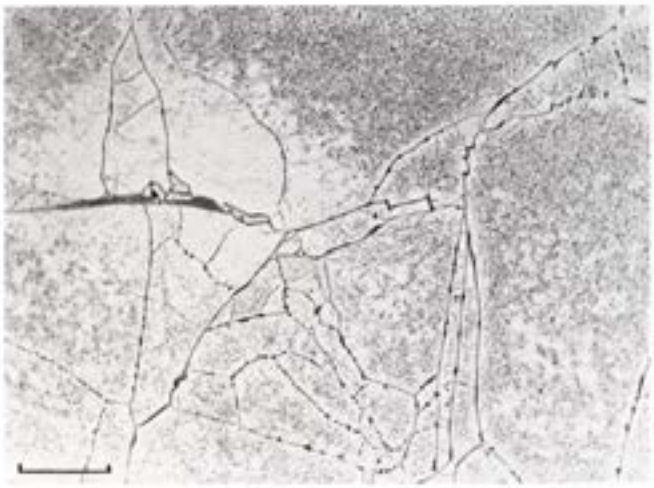

Figure 96. Smithville (Copenhagen no. 1876, 2244). The kamacite in numerous iron meteorites is rich in precipitates. Here, grain boundaries, subboundaries and defects of the grain interior have become decorated with phosphides. The particles of the interior are smallest (< 1 μ) and most densely spaced because they formed at the lowest temperature. Etched. Scale bar 300 μ.

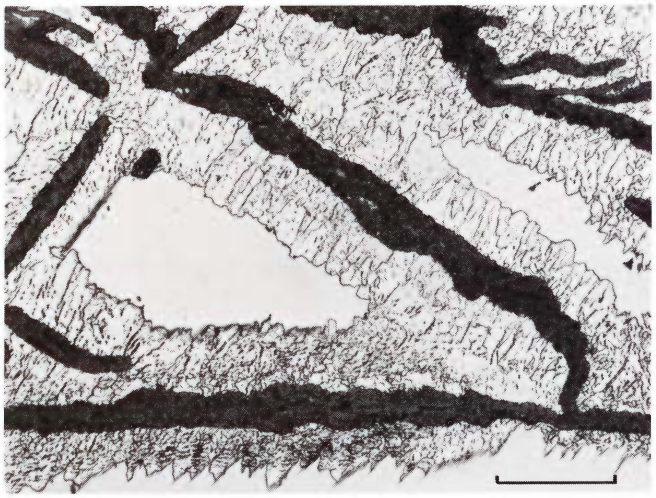

Figure 97. Wichita County (Copenhagen no. 1905, 1743). Cosmic annealing has decomposed the cohenite (white) to columnar ferrite grains (gray) and lamellar graphite (black). The decomposition started along microfissures in the cohenite. Etched. Scale bar 100 μ.

Figure 98. Bischtübe (Copenhagen no. 1903, 1362). Swathing kamacite around a schreibersite skeleton crystal. The swathing kamacite is about twice the width of the Widmanstätten lamellae. Significant grain growth on part of the swathing kamacite has occurred later. Etched. Scale bar 3 mm.

ously to the familiar Widmanstätten structure. The orientation of the swathing kamacite, which may often be composed of several grains, is usually unrelated to the Widmanstätten structure, which abuts unconformingly against it.

Neumann bands (Neumann 1850; Böggild 1927; Paxton 1953; Barrett & Massalski 1966: 407) are mechanical, plate-shaped twin lamellae in the kamacite. They occur in hexahedrites, octahedrites and even in ataxites as long as there is a coherent kamacite phase of more than 20-50 μ in width. The Neumann bands are narrow ($\sim$1 μ) in precipitate-rich kamacite, but reach widths of over 10 μ in pure kamacite of the same meteorite. They attain lengths of several centimeters in hexahedrites. The twin plane is $\{211\}_{\alpha}$ so it is possible to have 12 differently oriented Neuman bands on an artitrary section plane through a single α-crystal. The majority of the Neumann bands are preatmospheric; they probably date from cosmic collisions which were remote in time and space. An insignificant portion may have been caused by the violent atmospheric deceleration and are then usually located in the strained kamacite immediately around cracks. Contrary to general statements, virtually no Neumann bands form upon impact with the ground.

While the Neumann bands were probably formed under complex stress-strain conditions when shock waves of less than 130 k bar passed through the meteoritic material, other structures are caused by heavier shock waves. Smith (1958), Heymann et al. (1965), Lipschutz (1968), and others have shown that the peculiar transformations of the α-phase that were observed in some meteorites – e.g., by Perry (1944), Nininger (1956), Maringer & Manning (1962) and Buchwald & Munck (1965) – could be synthesized in the laboratory by exposing meteorites to shock pressures above 130 k bar. The peculiar crosshatched structure which

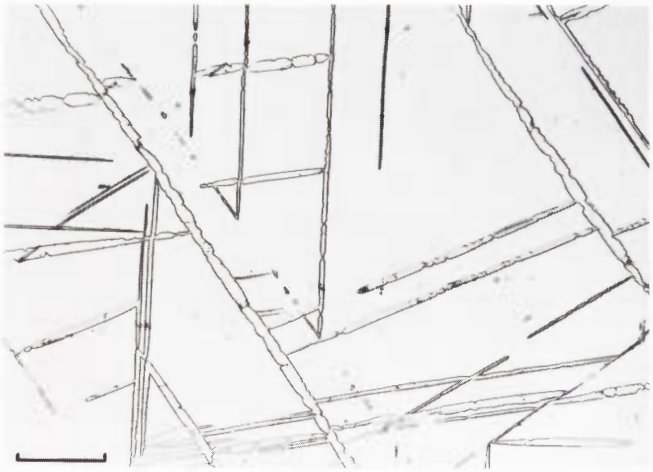

Figure 99. Silver Crown (U.S.N.M. no. 522). Typical Neumann bands in a kamacite lamella of a coarse octahedrite. Seven directions are clearly visible on this section. Etched. Scale bar 40 μ.

bears some resemblance to martensite is attributed to a temporary conversion of α-iron to hexagonal ϵ-iron, which is the stable iron modification above 130 k bar at room temperature. See Figure 104.

Reheating of the deformed and shock deformed kamacite causes stress relief, recovery, polygonization, recrystallization and grain growth (Leslie et al. 1962). The precise result will depend upon several factors, the most important being the degree of prior deformation, the annealing temperature, the Ni and P content of the kamacite, the annealing time, the heating rate and the number of inclusions. A thorough discussion of the very interesting effects will be presented elsewhere, let it suffice here to say that the effects are most conveniently followed by accurate microhardness measurements and observations of the associated structural changes. The structural changes may be followed by classical optical microscopy, by electron microscopy and by X-ray analysis. A meteorite

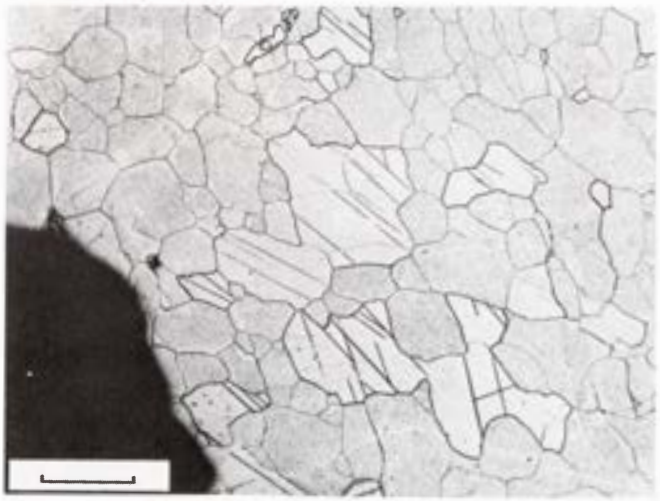

Figure 100. Zerhamra (Copenhagen 1972, 1680). The kamacite phase recrystallized in Cosmos and any original Neumann bands were wiped out. New Neumann bands formed in limited amounts close to fissures that opened during the atmospheric deceleration. Etched. Scale bar 300 μ.

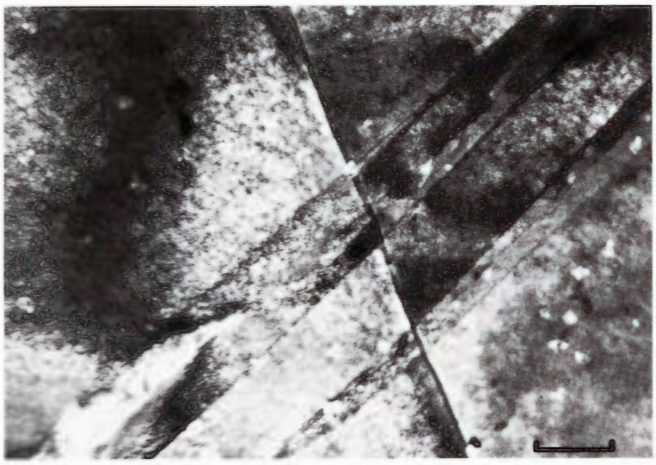

Figure 101. Cape York (Copenhagen no. 1967, 410). The figure shows two Neumann bands crossing a low angle boundary between two ferrite subgrains. Evidence of the high dislocation density in the matrix is seen on both sides of the boundary. Scale bar 2 μ. Transmissionelectronmicrograph.

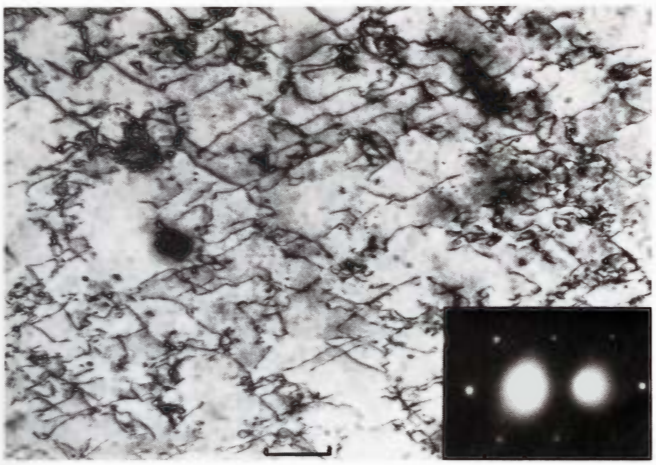

Figure 102. Cape York (Copenhagen no. 1967, 410). Dislocation segments in $\{111\}$ foil plane aligned parallel to two $<112>$ directions. A third dislocation, running almost vertically in the picture, is out of contrast. Scale bar 0.2 μ. Transmissionelectronmicrograph.

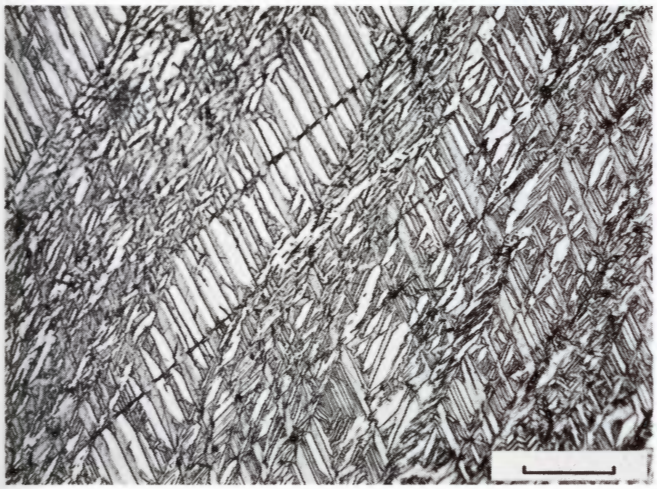

Figure 103. Ilimaes (Brit. Mus. no. 67450). Crosshatched kamacite of high contrast and of high hardness (275 Vickers), presumably caused by shock transformation $\alpha \rightarrow \epsilon$. Etched. Oil immersion. Scale bar 20 μ.

may ultimately be structurally altered almost beyond recognition (Bingera, Willamette) as the result of recrystallization and grain growth in the kamacite.

Kamacite shows cubic cleavage. This fact may easily be observed on old hand specimens of Braunau and other hexahedrites which have been split by hammer and chisel by their early owners. The cubic cleavage is, of course, not restricted to hexahedrites. The kamacite lamellae of octahedrites often display fine cubic cracks (Figure 105) which are evidently of preatmospheric origin and are often located deep inside the meteorite. They probably date from remote cosmic collisions.

Annealed or recovered kamacite has a hardness which is proportional to the amount of nickel and phosphorus in solid solution. Kamacite with 1.5% Ni has a Vickers hardness (100 g load) of 110±10, kamacite with 5.5% Ni 145±10, and kamacite with 7.0% Ni 155±10 (P is assumed constant at 0.15%; with about 0.05% in solid solution and 0.10% as phosphides). If the kamacite is subjected to plastic deformation, either as a result of slow cold work or of explosive shock loading, its hardness increases significantly. Kamacite with 7.0% Ni and with shock-produced Neumann bands displays a hardness range of 170-250; this kamacite, if still more effectively damaged by shock loads above 130 k bar, displays hardnesses of 320±30, and a hatched ϵ-structure. In fact, the microhardness together with the microstructure may, after calibration, be used to deduce the unknown shock pressures to which the material was once exposed.

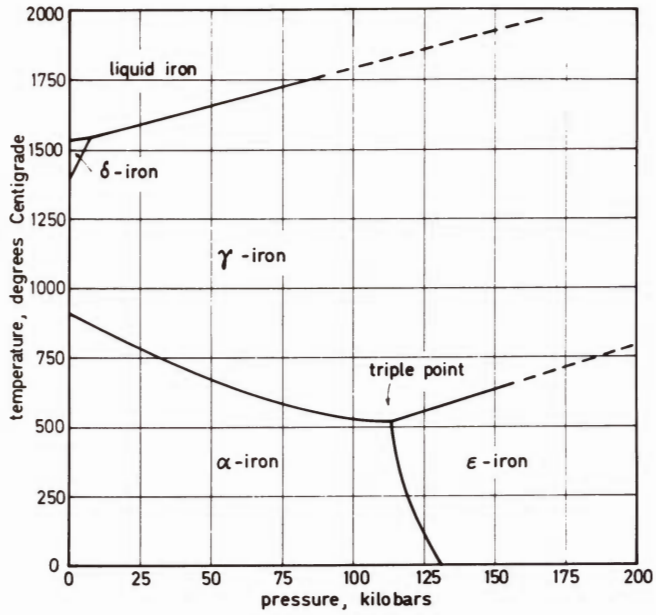

Figure 104. The phase diagram of pure iron shows where the various forms of iron are stable. α and δ are body centered cubic, γ is face centered cubic and ϵ is hexagonal close packed. At 25° C and 1 atmosphere the density of iron is 7.86 g/cm^3. At pressures up to 130 k bar the density increases gradually to 8.46. When the α-phase here transforms to ϵ, the density abruptly jumps to 8.81. Thereafter, as the pressure is further increased, the density again increases uniformly and reaches 9.10 at 200 k bar. (From Takahashi & Bassett 1964.)

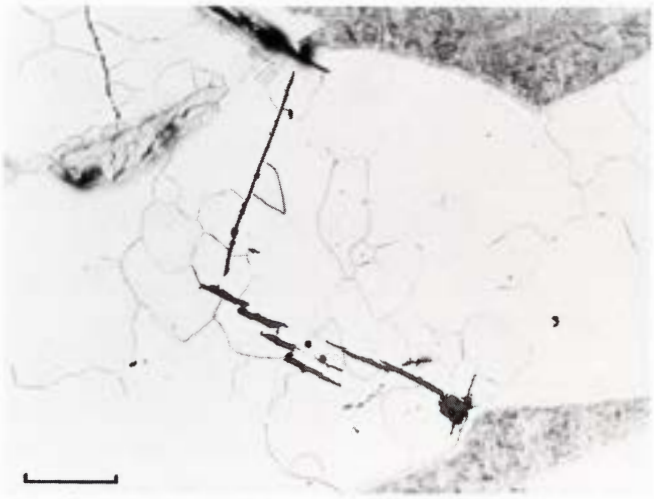

Figure 105. Joel's Iron (Brit. Mus. no. 35782). Recrystallized octahedrite. The fine fissures – now partly filled with terrestrial corrosion products – follow the cubic cleavage planes of the original kamacite lamella. The subsequently formed recrystallized grains have been limited in their growth by the fissures. Etched. Scale bar 200 μ.

Taenite. When face centered cubic austenite – with more than 25% Ni in solid solution – occurs in meteorites, it is called taenite. The word is derived from the Greek *tainia*, meaning band (Reichenbach 1861). In octahedrites the taenite forms three-dimensional sheets or lamellae that appear band-shaped in sections. In special circumstances, taenite occurs in hexahedrites, particularly if these have been subjected to secondary reheating with unequilibrated structures as a result. See, e.g., Wathena and Mejillones. Taenite is a major component of group IVB and almost fully makes up the composition in San Cristobal, Twin City, and Santa Catharina.

The taenite is variable in composition with respect to Ni (25-50%), Co (0.3-0.8%), C (0.05-0.5%?) and P (0.05-0.1%). Electron microprobe traverses across kamacite, taenite and plessite (Feller-Kniepmeyer & Uhlig 1961; Wood 1964; Reed 1965b; Massalski et al. 1966) have shown that the taenite has a high (30-50%) nickel content where it abuts on kamacite and trails off to less than 25% where it grades into the various plessite varieties.

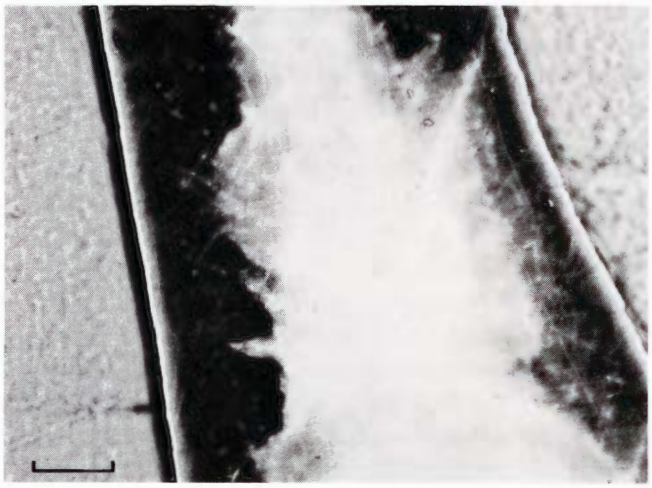

Figure 106. Cape York (Agpalilik) (Copenhagen no. 1967, 410). A 50 μ wide taenite lamella which displays the usual features of taenite in unannealed meteorites. A 1-2 μ wide yellow rim, a cloudy transition zone that stains in brown-blue colors, and a yellowish interior. All zones contain more than 30% Ni, the rims, with 40-50% Ni, being richest. Etched. Scale bar 10 μ.

The taenite inhomogeneity, which has now definitively been proved with the powerful electron microprobe, has long been suspected and has also been semiquantitatively examined by classical analytical methods (e.g., Cohen 1894: 99; Johnston & Ellsworth 1921).

Microhardness testing and optical examination of unannealed taenite (for example a group IIIA iron) clearly indicate the inhomogeneities. Traversing from the kamacite-taenite interface inwards, a 1-2 μ wide creamcolored taenite (50-40% Ni; hardness not measurable) is first encountered. Then follows a 5-25 μ wide bluish-brown stained zone (40-30% Ni; HV $\sim$ 350) and a 10-30 μ wide yellow zone (30-25% Ni; HV $\sim$ 400). These two zones are usually intergrown, and light subboundaries are visible in the taenite. Minute schreibersite grains are sometimes embedded in the taenite.

Next follow yellowish zones, 20-50 μ wide, with indistinct martensitic transformation products (< 25% Ni; HV $\sim$ 450-500) and then distinctly brown-etching zones where martensite platelets are developed parallel to the bulk Widmanstätten structure (<20% Ni; HV $\sim$ 350-400). Finally, various plessitic varieties occur; see below.

The dark stained taenite of Yenberrie and Cape York was studied with a carbon replica method. Electron microscopy revealed the dark patches to contain a large number of densely spaced etch-pits, channels and grooves that enveloped unattacked islands. It appears that the Nital etchant had dissolved a kamacite component and left a high-nickel taenite component unattacked. That is, the stained taenite may be interpreted as a submicroscopic two-phase mixture wherein cell walls of kamacite enclose small volumes of taenite (0.1-0.4 μ across). Similar results have been reached independently by Scott (1972; personal communication).

Densely spaced sliplines parallel to $\{111\}_\gamma$ are often present in the dark-stained taenite and the yellow taenite. See Figure 110. They have been reported once before (in Grant; Maringer & Manning 1962) but are apparently quite common in shocked meteorites. The detection requires well polished, or electropolished samples, and an oil immersion objective.

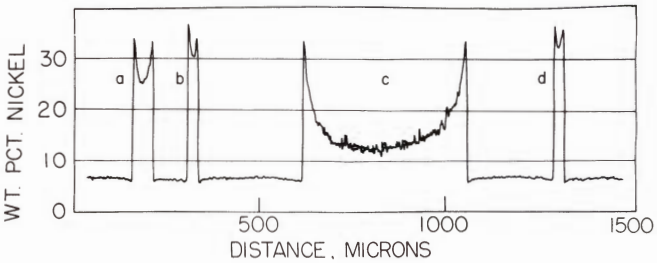

Figure 107. The so-called M-curve for taenite and plessite. Electron microprobe traverse across narrow taenite lamellae, like Figure 106, (b, d), and duplex regions (a, c). (From Wood 1964.)

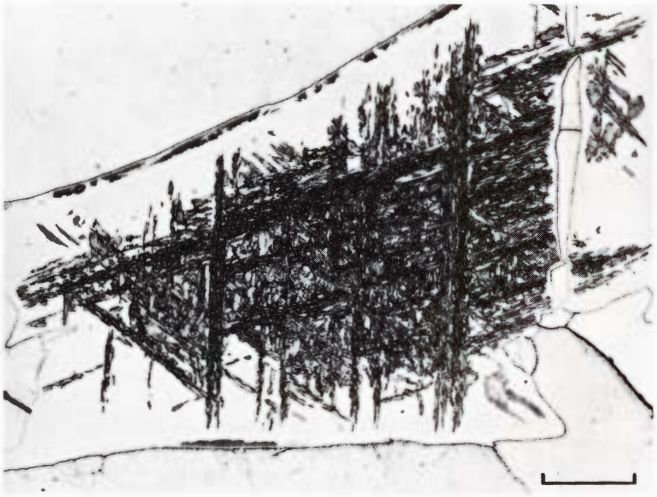

Figure 108. Tamentit (Copenhagen 1972, 1686). When the retained taenite fields are more than about 50 μ wide, the interior portions, with about 20-25% Ni, decompose in a martensitic pattern parallel to the bulk Widmanstätten pattern. It is typical of many fields in group IIIA, IIIB, IID and I. The morphology resembles that of nickel-martensite produced upon rapid cooling followed by some tempering. As applied here, the term martensitic is purely descriptive and does not imply formation as the result of rapid cooling. Etched. Scale bar 100 μ.

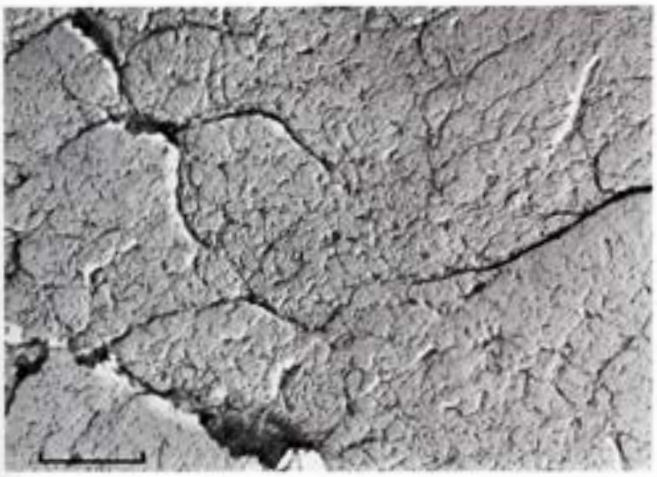

Figure 109. Yenberrie (U.S.N.M. no. 607). Electron micrograph of a carbon replica shows cloudy taenite to be a submicroscopic two-phase mixture of kamacite (etch pits) and taenite. Scale bar 2 μ.

The hardness variations discussed here are typical. While the hardness numbers will vary from meteorite to meteorite – depending on the degree of deformation, shock and annealing, – the trend is always the same: the taenite is significantly harder than the kamacite. See Figure 111. This is contrary to general statements advanced by, e.g., Perry (1944: 14) who believed taenite and kamacite to have equal hardness. This is only true under certain circumstances, mainly when both phases are fully annealed (Buchwald 1971d). The maximum hardness observed is 355 for kamacite but 585 for taenite. Values above 450 are particularly common in the martensitic decomposition zones of the carbon-rich taenites of group I (Toluca, Canyon Diablo, Youndegin, Odessa). The high hardnesses

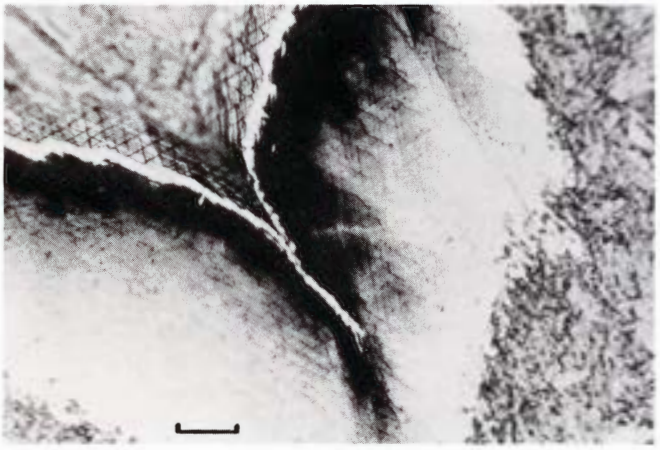

Figure 110. Veliko-Nikolaevskij Priisk (Moscow no. 761). The slip-lines which are indistinctly visible in the taenite of Figure 106 are better developed here. The Nital etchant has removed part of the kamacite in the upper left corner so that the slipline traces on the sloping taenite surface become clearly visible here. Oil immersion. Scale bar 10 μ.

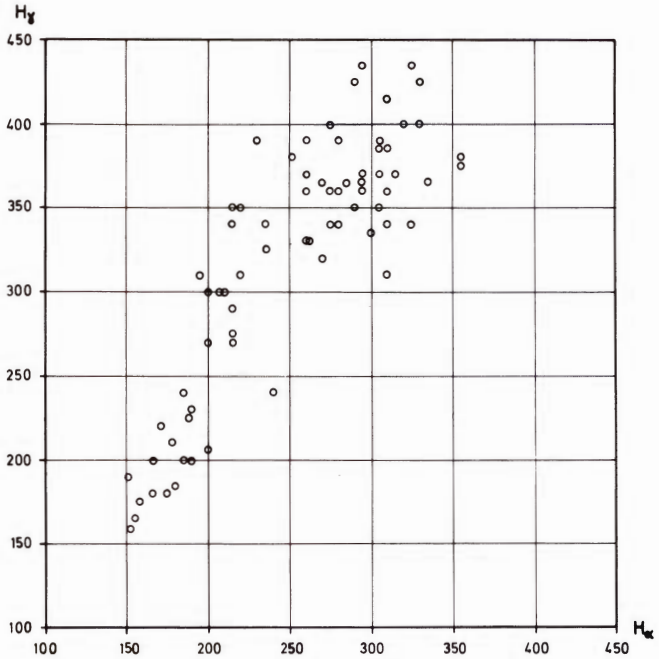

Figure 111. The microhardness (100 g Vickers pyramid number) of the kamacite and taenite are correlated, the taenite always being harder. Each circle represents the average of several measurements from one meteorite. Kamacite numbers are the average of ten, taenite numbers of five measurements within the same polished section.

of the taenite are mainly due to plastic deformation and particularly to shock deformation.

Odessa specimens subjected to artificial shock pressures up to 1,000 kilobars clearly show intensive shock hardening of the taenite. See Figure 112. Remarkable is the steep beginning of the curve and the more moderate increase at higher shock intensities. Also remarkable is the fact that a maximum occurs on the kamacite curve at about 200 k bar. The relaxation heat associated with higher shock intensities evidently suffices to anneal, recrystallize and transform the

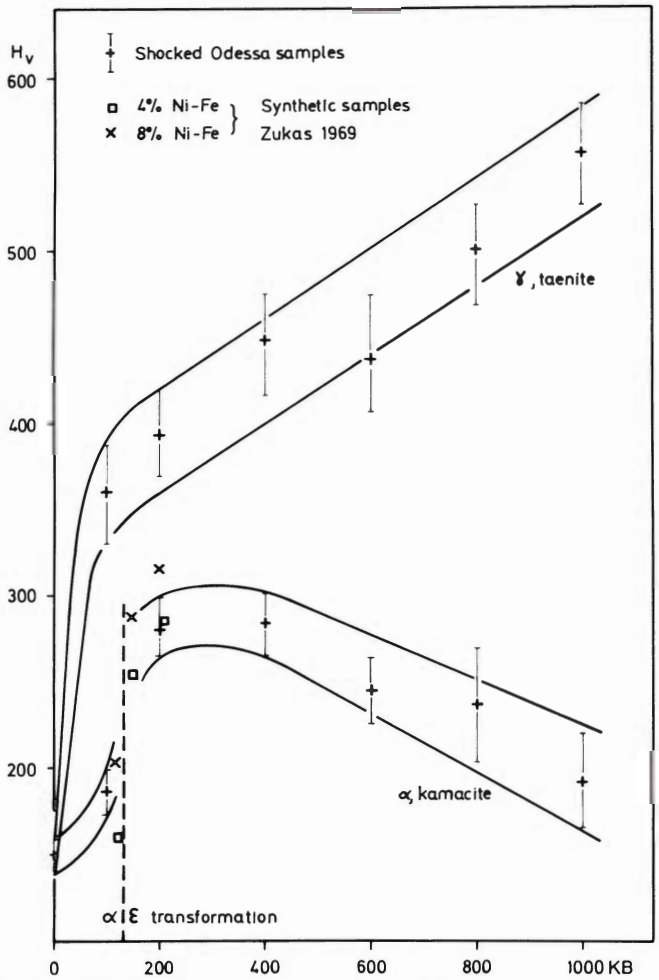

Figure 112. Calibration curves for shocked kamacite and taenite. The shocked Odessa samples were provided by Dr. Robin Brett, NASA, Houston, and measured by the author. Data on synthetic alloys are from Zukas 1969. All data are, due to natural scatter and steep pressure gradients in the shocked samples, given as hardness bands.

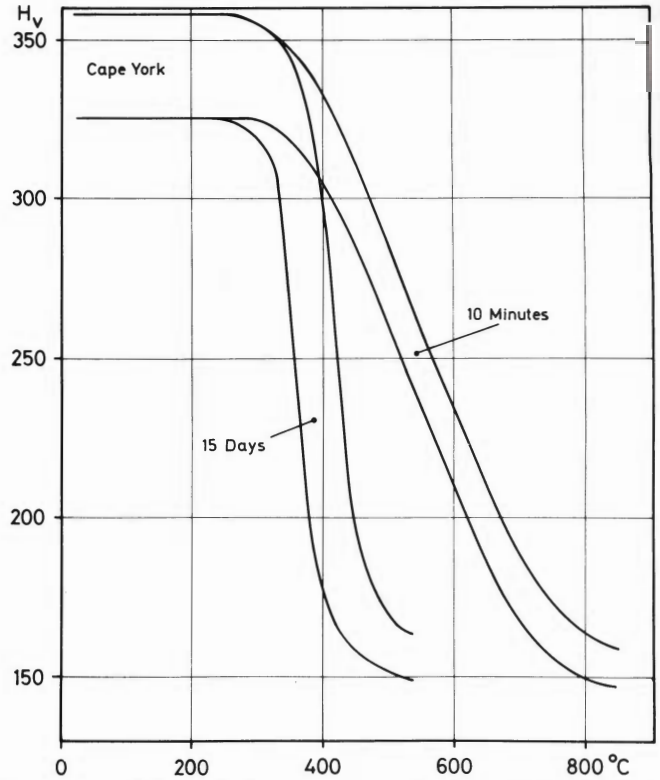

Figure 113. Moderate heat treatments will anneal cold-worked taenite to hardnesses of 155±5. Few structural changes are observed before the temperature increases above 500° C.

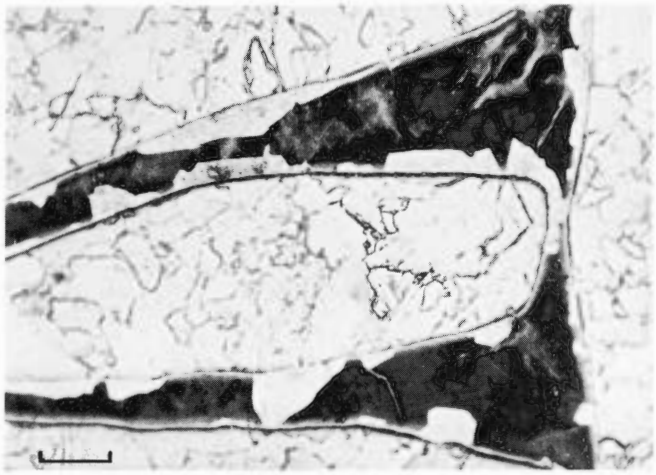

Figure 114. Kayakent (Copenhagen no. 1973, 2082). Atmospheric heating of the taenite lamellae has caused the sharp high-nickel edge of the cloudy taenite to advance irregularly towards the interior. The kamacite shows α_2 structure. Peak temperature was 900° C for a few seconds. Etched. Scale bar 20 μ.

kamacite (to α_2), while taenite under the same conditions still acquires more shock hardness. These observations have been used extensively in the book – together with observations of troilite and cohenite – in order to form a faceted picture of the shock history of iron meteorites. See, e.g., Canyon Diablo.

Annealing softens the taenite. Fifteen days at 500°, 10 minutes at 800°, or 10 seconds at 900° C develop minimum values of about 155. See Figure 113. These relatively mild reheatings produce two pronounced structural effects. The stained– and strained–taenite is replaced by soft yellow structureless taenite; i.e., the submicroscopic $\alpha + \gamma$ mixture is homogenized to taenite. If the annealing is imperfect, a peculiar mosaic appearance with yellow patches becomes visible (See Figure 114.); the yellow patches increase in size, often in a very curious way, and develop straight interfaces. The second effect is visible whenever appreciable carbon is in solid solution in the taenite. The reheating enables carbon to diffuse 10-30 μ out into the surrounding kamacite. Since this is taenitic at the reaction temperature, subsequent cooling produces bainitic-martensitic zones with considerable hardness (~ 300) along the taenite rims. The reactions thus result in a complete inversion: dark and hard taenite becomes light and soft, while the opposite effect is apparent in the adjacent kamacite.

Thorough annealing decomposes and spheroidizes the taenite. See Figure 115 and Hammond, Maria Elena, Willamette and Zerhamra. In extreme cases, such as Juromenha and Smithland, the original taenite bands and plessite fields are no longer recognizable at all. See Figure 116.

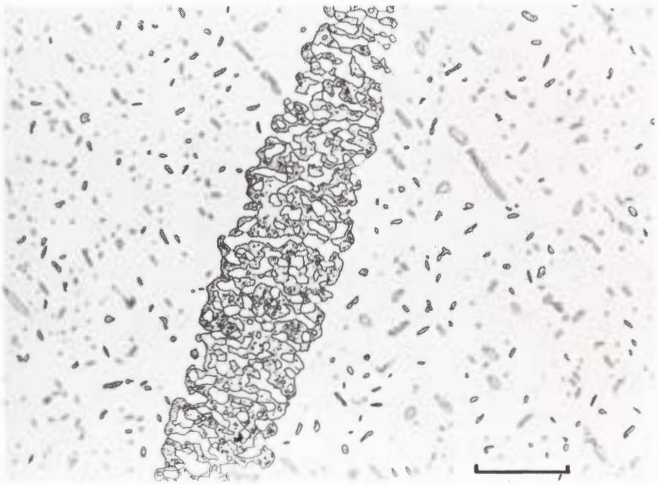

Figure 115. Thoroughly decomposed taenite lamella and spheroidized γ-particles in kamacite. The structure indicates severe cosmic annealing and is present in, e.g., Maria Elena and Seneca Falls. Etched. Scale bar 40 μ.

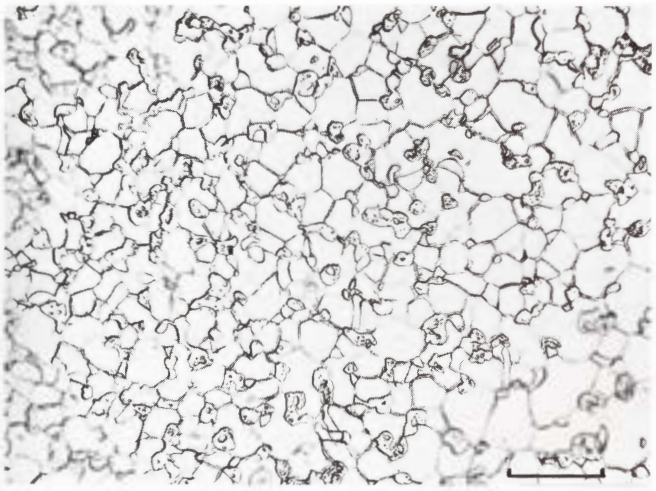

Figure 116. Juromenha (U.S.N.M. no. 3534). An extreme case of a cosmically reheated structure. The taenite lamellae are entirely decomposed and spheroidized to 5-10 μ blebs (spotted). Phosphides occur as slightly smaller, angular blebs (white). The matrix is polycrystalline kamacite. Etched. Scale bar 40 μ.

Plessite. Plessite is not a mineral. It is a somewhat ambiguous term that traditionally has covered things that are neither kamacite nor taenite but a mixture of both phases. Basically, plessite is the two-phase mixture of α and γ that is the last to develop from the retained taenite during continuous primary cooling. Plessite may, however, also form by the two stage reaction $\gamma \rightarrow \alpha_2 \rightarrow \alpha + \gamma$. In this, the cooling austenite transforms initially diffusionless to α_2, whereupon α_2 isothermally or by mild reheating decomposes to $\alpha + \gamma$. The plessite fields are usually framed by a continuous taenite rim, and they usually display concave outlines towards adjacent kamacite.

When better microscopes and analytical methods were introduced, it was discovered that plessite could assume a multitude of forms; consequently very many descriptive terms have been introduced. Some of the more commonly used have been discussed by Reichenbach (1861), Cohen (1894: 104), Perry (1944: 15), Zavaritskij & Kvasha (1952: 20) and Massalski et al. (1966).

In this work various main forms are recognized. These are important because they – with few exceptions – can be referred to distinct chemical groups and no doubt will ultimately be of use when deducing cooling rates and reheating events.

Pearlitic plessite (See Figure 118) is a term used to describe a lamellar intergrowth of α and γ. The taenite lamellae are usually 0.5-2 μ wide, but electron microscopy has revealed still finer lamellae and also indicates a relationship to the stained taenite above with which it is often associated. The pearlitic plessite is characteristic of group I (e.g., Canyon Diablo) and appears to be dependent upon carbon for its formation. It also occasionally occurs in

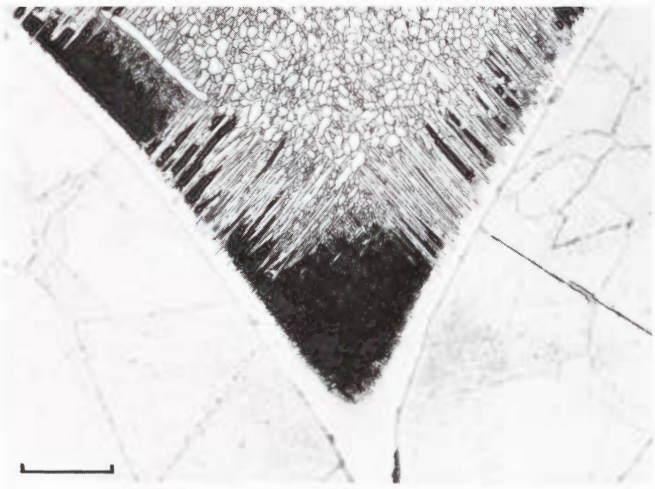

Figure 117. Cape York (Agpalilik) (Copenhagen no. 1967, 410). Typical plessite field, displaying great structural variety within one field. The surrounding kamacite has subboundaries, Neumann bands and a few cracks (lower right) along the cubic cleavage planes. Etched. Scale bar 200 μ.

Figure 118. Mazapil (Chicago no. 1977). Pearlitic development of the plessite is typical of carbon-containing group I meteorites. The 1-2 μ wide lamellae are taenite. To the right is massive cloudy taenite. Near the scale bar a 20 μ schreibersite crystal. Etched. Scale bar 20 μ.

cosmically annealed irons of other groups. It is always softer than the taenite from which it formed.

Spheroidized plessite (See Figure 120) consists of kamacite in which 1-20 μ spherulitic taenite particles are unevenly dispersed. It occurs together with pearlitic plessite, particularly in group I. Carbides, such as haxonite, are often precipitated around the spherules and the lamellae of spheroidized and pearlitic plessite, respectively. See Figures 143 and 144A.

Acicular plessite, Figures 121-122, is a basket weave intergrowth of pointed α-platelets with retained and often stained taenite. The α-spindles repeat the bulk Widmanstätten pattern and are usually 1-10 μ wide. This plessite variety is also particularly common in group I, e.g., Toluca.

Comb plessite, Figure 123, has been called perthitic plessite by Zavaritskij & Kvasha (1952) and Krinov

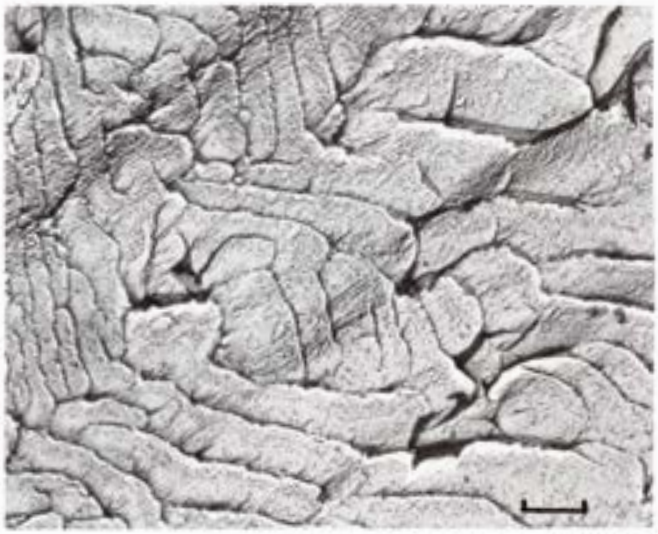

Figure 119. Yenberrie (U.S.N.M. no. 607). Electron micrograph of a carbon replica through a number of sloping taenite lamellae of a pearlitic intergrowth. Etched. Scale bar 1 μ.

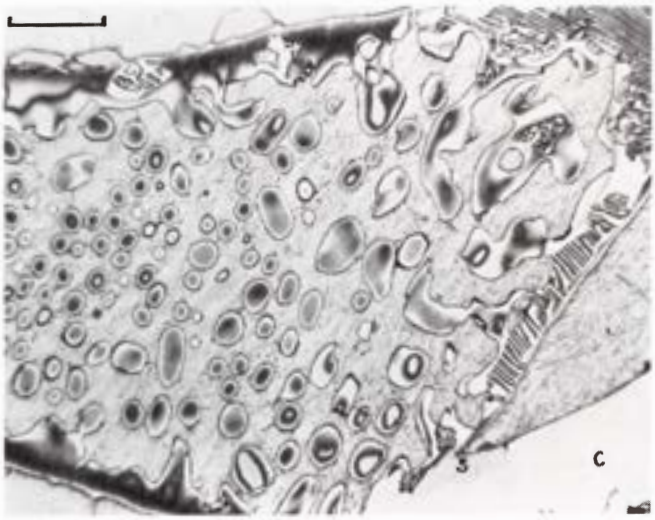

Figure 120. Canyon Diablo (Copenhagen no. 17270). Spheroidized plessite associated with pearlitic plessite within the same field. Cloudy taenite is prominent. Below right cohenite (C) and schreibersite (S). Etched. Scale bar 40 μ.

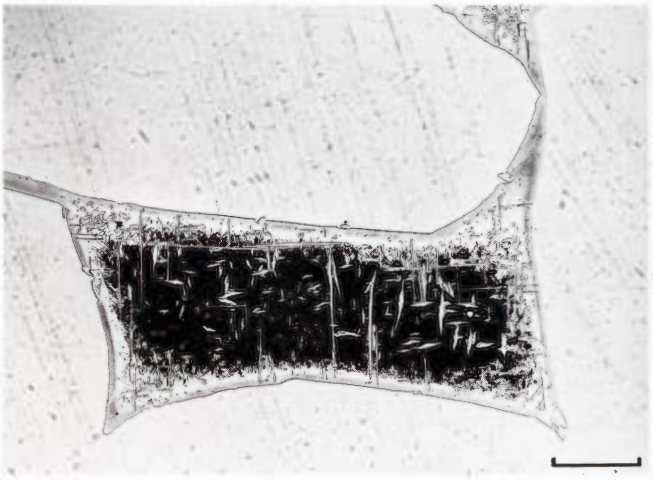

Figure 121. Goose Lake (U.S.N.M. no. 1332). Acicular plessite in a typical modification. Etched. Scale bar 200 μ. (Perry 1950: volume 6.)

Figure 122. Pan de Azucar (The Carrizalillo specimen in Oslo). Acicular plessite in a coarser development than Figure 121. Two large schreibersite particles are marked S. Etched. Scale bar 50 μ.

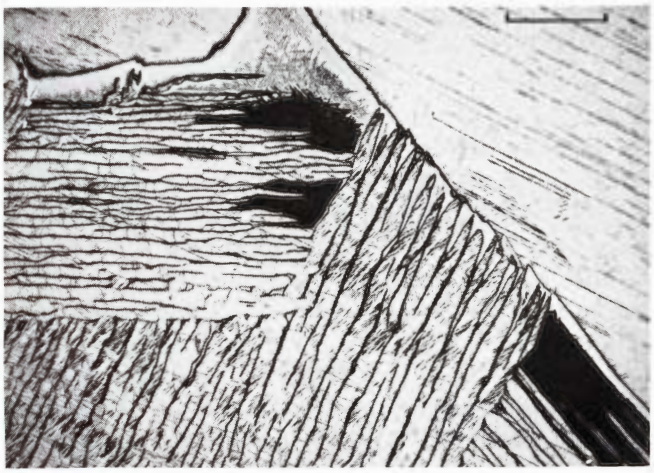

Figure 123. Spearman (Tempe no. 230.3). Large plessite fields are often developed as comb plessite. Other varieties are almost always present in minor amounts. All kamacite is of the shock-hardened ϵ-variety. Etched. Scale bar 400 μ.

(1960a: 331). The narrow taenite ribs radiate inwards from a more or less continuous taenite frame and indicate the bulk Widmanstätten orientations.

Net plessite, Figure 124, is very closely related to comb plessite and is sometimes just a section perpendicular to the comb plessite. The taenite appears as 1-10 μ islands in a kamacite which is rich in boundaries and subboundaries. Comb and net plessite are particularly common in groups IIIA-IIIB but also occur in I, IIC, IID, IIIC and IVA. Schreibersite particles 1-50 μ in size, are quite common inside the fields, substituting for taenite particles of similar sizes.

Cellular plessite, Figure 125, is an open-meshed aggregate of α-grains (cells) within a continuous taenite frame. Each α-grain is differently oriented and contains numerous tiny oriented γ-particles. The cellular plessite is typical of group IVA, e.g., Gibeon and Chinautla, and rare in other groups.

Finger plessite, Figure 126, is a variety of cellular plessite, with more taenite and with strong Widmanstätten orientation. It also mainly occurs in group IVA.

Black plessite and *black taenite*, Figure 127, are terms used to distinguish small wedge-shaped fields and transitional zones that, even after light-etching with nital, are severely attacked and appear black and unresolvable under the microscope. The appearance is caused by the selective dissolution of the finely dispersed α-component which is less than 0.5 μ in size.

Duplex plessite and *duplex $\alpha + \gamma$ mixtures*, Figure 128, are terms used for the transitional zones in large plessite fields. They have 12-18% Ni on the average and display intricate intergrowths of ½-2 μ α- and γ-particles. There are subboundaries in the α-phase, and the γ-particles may

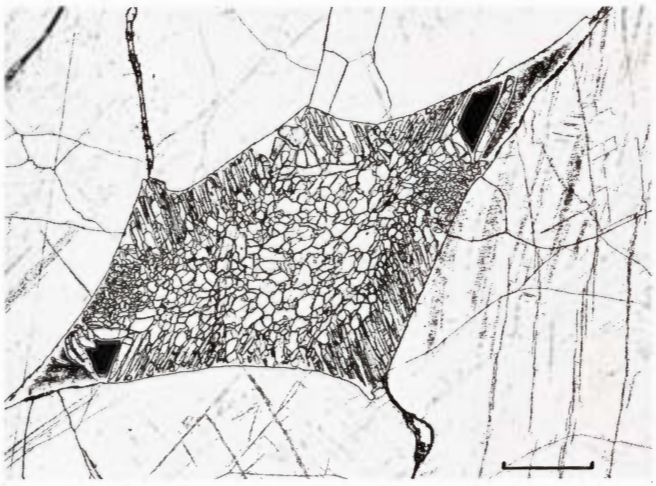

Figure 124. Trenton (U.S.N.M. no. 668). Typical net plessite. Other varieties are present in minor amounts. All kamacite is of the shock-hardened ϵ-variety but appears slightly different from that in Figure 123. Etched. Scale bar 400 μ. (Perry 1950: volume 5.)

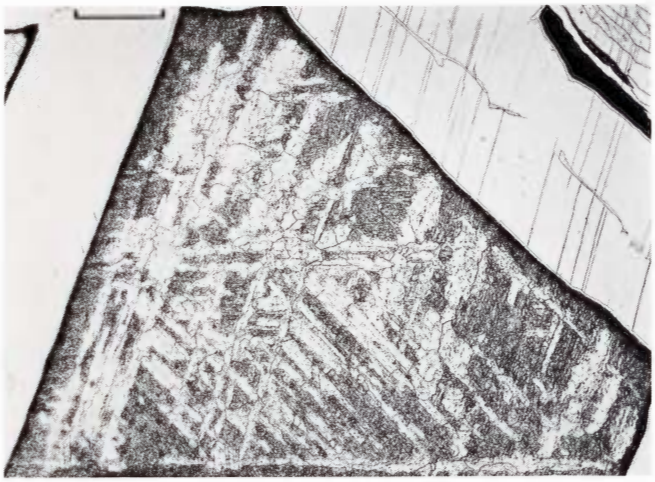

Figure 126. Bushman Land (U.S.N.M. no. 2515). Finger plessite. Large plessite fields of group IVA are aften subdivided in elongated kamacite grains that follow the Widmanstätten directions. The exsolved taenite particles are very small. Etched. Scale bar 200 μ.

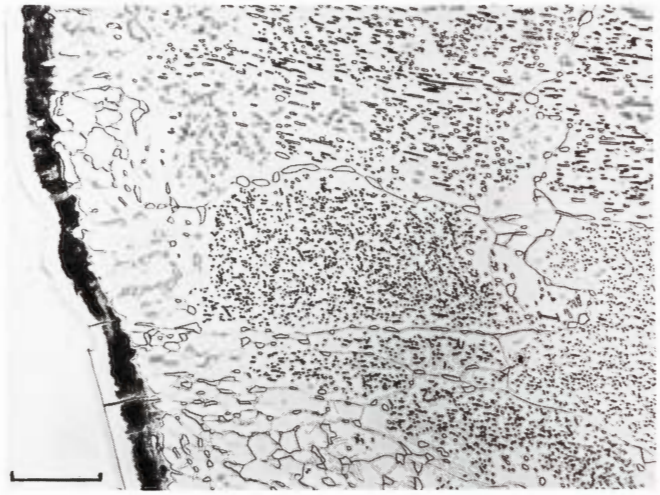

Figure 125. Chinautla (Copenhagen no. 1913, 199). Cellular plessite. The plessite field has a frame of taenite to the left. The interior is subdivided in grains of different orientation, with γ-precipitates along the grain boundaries and in the interior. Etched. Scale bar 100 μ.

Figure 127. Kouga Mountains (Brit. Mus. no. 1916, 60). Black taenite or black plessite, here developed as a transitional zone between clear taenite and duplex plessite of the interior. Also an "island arc" of schreibersite particles. Etched. Scale bar 50 μ.

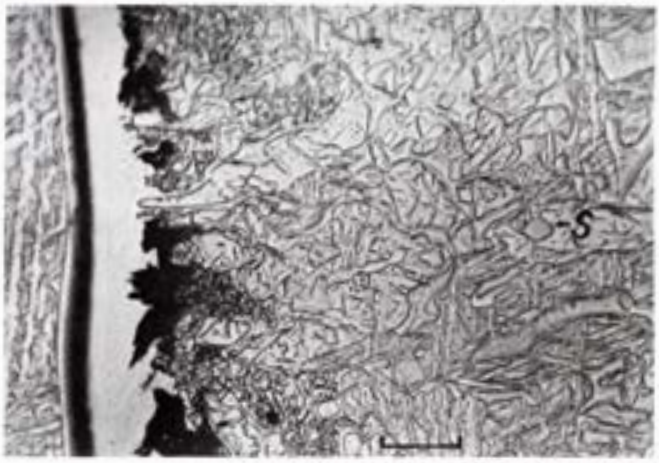

Figure 128. Wallapai (Tempe no. 58bx). To the right, rather coarse-grained duplex plessite. The kamacite part is of the shock-hatched variety. A schreibersite particle is marked S. To the left, a cloudy taenite and a black transition zone. Etched. Scale bar 20 μ.

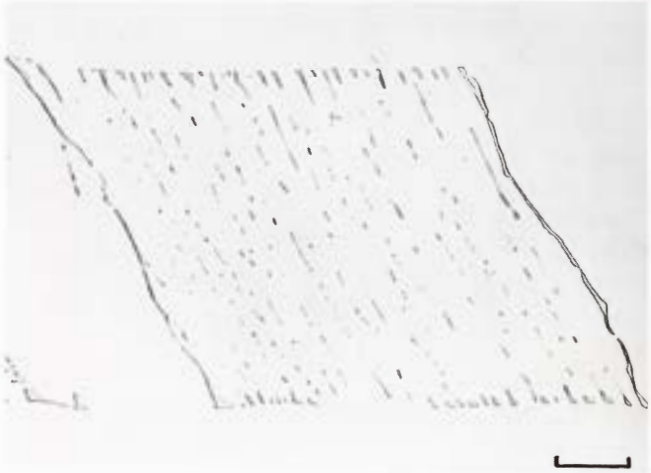

Figure 130. Henbury (Copenhagen no. 1939, 84). Degenerated comb plessite. Typical for many medium octahedrites of the low-Ni, low-P end of group IIIA. Slightly etched. Scale bar 500 μ.

themselves be decomposing on an almost submicroscopic scale to $\alpha + \gamma$; compare the stained taenite. The bulk of many ataxites, such as Iquique, Figure 129, is made up of duplex plessite. Perry (1944) called this structure para-eutectoid plessite, but the term has not been widely used.

Degenerated plessite, Figure 130. Any of the above forms, but particularly the comb-, net- and cellular varieties may be degenerate; i.e., imperfectly developed, usually because the bulk nickel value for the whole meteorite is so low that most of the taenite has disappeared after full primary cooling.

Altered plessite. All of the above varieties will be significantly changed on reheating, either in space or artificially. Thorough reheatings tend to perforate the taenite bands and create intricate, polygonized α-γ intergrowths. See Figure 131. Artificial, imperfect reheatings tend to produce blurred and diffuse taenite, from which P-rich thorns and spikes may protrude along the kamacite grain boundaries. See Figure 132.

A complete traverse with the electron microprobe across a plessite field usually shows a distinct M-profile (See Figure 107); i.e., the nickel varies systematically from high values (30-50%) at the taenite edge to low values (8-20%) in the two-phase interiors. The detailed examination of such M-profiles has enabled Wood (1964), Short & Andersen (1965), Goldstein & Short (1967a), Goldstein (1969) and Powell (1969) to estimate the cooling rates of iron meteorites and of meteorites with significant iron inclusions. They found that the latter part of the primary cooling, when the Widmanstätten structure formed between 700° and 300° C, occurred under almost isothermal conditions. They arrived at cooling rates that ranged from 0.1° C per 10^6 years (mesosiderites) through 0.5° C per 10^6 years (Butler, Laurens County; pallasites) to 500° C per 10^6 years (Deep Springs, Monahans, Arltunga).

Since the author feels that the absolute values for the cooling-rates are still uncertain, no cooling-rates are quoted under the individual descriptions. The interested reader

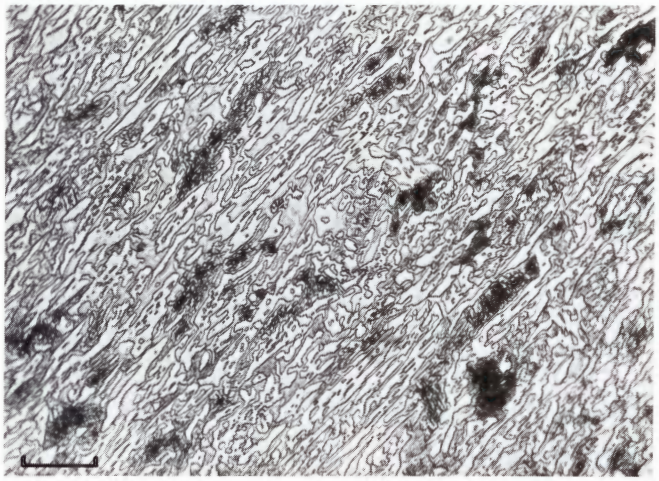

Figure 129. Iquique (Berlin). Typical duplex plessite of an ataxite of group IVB. Within square centimeters there is a homogeneously oriented sheen because the α- and γ-particles are aligned in preferred directions. Etched. Scale bar 20 μ.

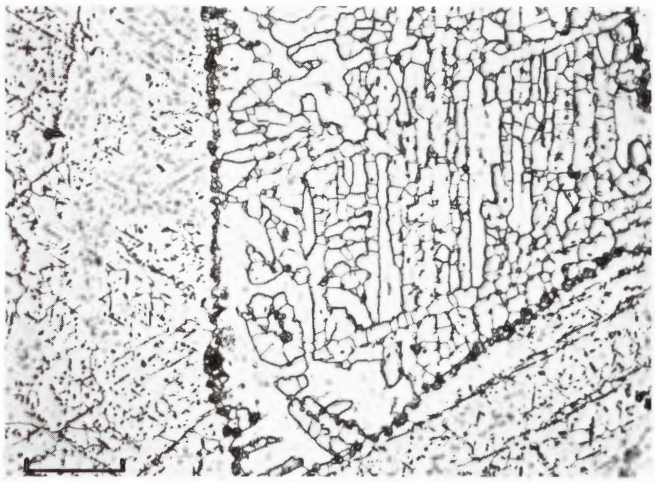

Figure 131. Maria Elena (U.S.N.M. no. 1221). Severely altered plessite field, caused by prolonged annealing in space. The kamacite lamellae are also altered, displaying oriented γ-precipitates. Etched. Scale bar 100 μ.

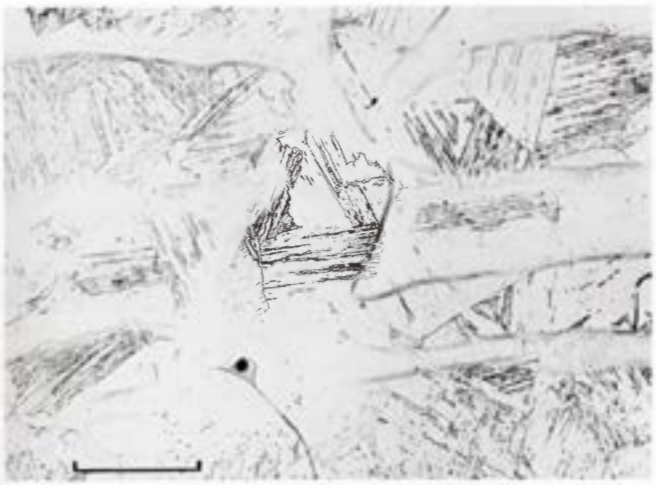

Figure 132. Prambanan (Chicago no. 1160). Short-term artificial reheating to 900°-1000° C has washed out the plessite fields, melted the troilite inclusion and caused unequilibrated α_2 structures to form on cooling. Etched. Scale bar 200 μ.

may, however, from the known Ni contents and kamacite bandwidths reported in this work, readily derive the cooling-rate for most octahedrites. This can be done, e.g., by application of the approximative methods developed by Short & Goldstein (1967) and Wasson (1971b).

Microhardness traverses across taenite and plessite show curves similar to the M-profiles (Buchwald 1961b), and microhardness data may, after calibration, be applied as a substitute for the microprobe. Some hardness data are tabulated in Appendix 1, columns 10-11. Many more are included in the individual descriptions. Care must always be taken to compare "equivalent" taenite, because a wide scatter will occur if taenite with steep Ni gradients is inadvertently included.

The hardness of the plessite varieties ranges from about 160 to about 325 when measured with a 100 g load and thus integrating over numerous $\alpha + \gamma$ particles. The hardness is determined by the α/γ ratio, and by the degree of strain present in the two-phase mixture and in the individual components. Cold-worked or shock-hardened dense plessite varieties attain maximum values of 300-325 (e.g., Chinga and Cape York), while similar plessite of annealed meteorites displays minimum hardnesses of 160-200 (e.g., Ternera and Durango).

The unequilibrated α_2 structure

The normally recognized kamacite, taenite and plessite morphologies are the result of exceedingly slow continuous cooling. Subsequent reheating and renewed cooling have often occurred in meteorites, but in most cases structural equilibrium was finally obtained. If, however, meteoritic nickel-iron is reheated into the austenitic region and then cooled relatively rapidly – i.e., within minutes or hours or even days – to room temperature, unequilibrated structures will develop.

The most important is the α_2 phase (Jones & Pumphrey 1949; Allen & Earley 1950) which forms diffusionless from nickel austenite by a martensitic reaction. It is a cubic phase that shows line broadening in an X-ray diffractogram. Under the optical microscope it appears as serrated blocks (See Figure 133), or, when the nickel percentage increases above 8-10%, acquires a characteristic plateshape. Within each parent austenite crystal the plates occur in a maximum of four directions, parallel to $\{111\}\gamma$, i.e., the habit plane coincides with the Widmanstätten plane. If a specimen is pre-polished and then cooled in a vacuum from austenite temperature to room temperature, e.g., by water quenching, the surface will display relief affects characteristic of bundles of fine plates. See Figure 134. Swanson & Parr (1964) and Speich & Swann (1965) have examined the conditions under which α_2 forms and have presented thin-film electron transmission photographs of the structures. They found α_2 to possess a high defect structure with dislocation cells and twin related laths.

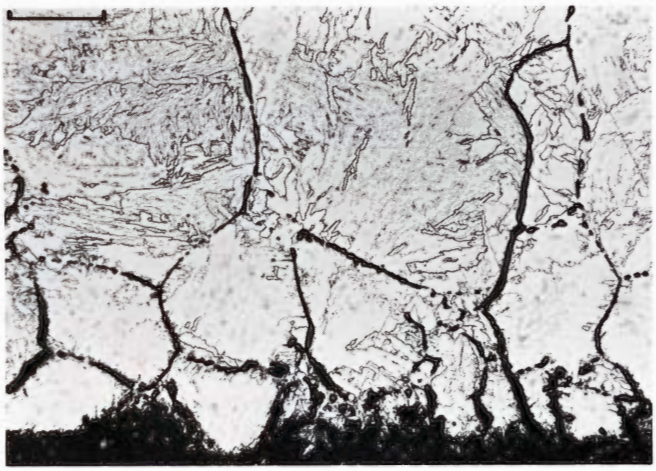

Figure 133. Cacaria (Tempe no. 19a). Typical α_2 structure in an artificially reheated meteorite. The temperature was briefly – for about an hour – above 800° C, and high temperature oxidation proceeded along austenite boundaries from the surface (below). Etched. Scale bar 200 μ.

Figure 134. Synthetic meteorite with 15% Ni, 0.5% P, balance Fe. Homogenized at 1100° C for 48 hours. Polished and then reheated to 900° in a vacuum hot-stage microscope. Upon cooling the polished surface acquired a distinct relief, differently oriented within each parent austenite grain. Scale bar 20 μ.

The martensitic α_2 structure is harder than the annealed α-phase and harder than the fine-grained ($\alpha+\gamma$) mixtures resulting from decomposition of the α_2 phase (Buchwald 1966). However, α_2 is tough and ductile and not as hard as might be expected if one is familiar with the similar appearing, but tetragonal, carbon-martensite of steels (Kelly & Nutting 1961). Phosphorus in solid solution increases the hardness of α_2 significantly, and so does carbon. These elements are, however, usually present at low levels (less than 0.5%).

The chemical composition of the α_2 phase is the same as that of the γ-phase from which it was formed by diffusionless transformation. It is thus possible to have α_2 phases of widely varying composition: the hexahedrites will form 5.5% Ni - α_2 (H ~ 170), the lamellae of coarse octahedrites will form 6.5% Ni - α_2 (H ~ 180) and those of medium octahedrites 7.5% Ni - α_2 (H ~ 190), to give a few general examples. The α_2 is present, with a hardness of 190±30, on all recent falls as a 2 mm wide rim zone. See Figure 135. Where the α_2 has formed by transformation of a kamacite which was previously shock-hardened, e.g., on Grant, Juncal and Merceditas, the α_2 units are usually fine-grained and reach their maximum hardness (~ 210±15). The α_2 phase is also a common component of artificially reheated and forged meteorites; compare Appendix 5. In meteorites which were thoroughly reheated, such as Cacaria and Prambanan, α_2 was formed through homogenization of preexisting fine-grained $\alpha + \gamma$ fields. The resulting α_2 phase may in such cases contain 12-20% Ni and attain a hardness above 250.

In many meteorites certain parts of the taenite and plessite fields may contain 28-32% Ni and 0.01-0.5% C; exposed to relatively rapid transformation, for example during the atmospheric flight or artificial reheating, such alloys may upon cooling produce prominent nickel-martensite with internal twinning. This martensite will have the habit plane $\{225\}\gamma$ and will often be located within conspicuous fields of retained austenite (Marder & Marder 1969). For other martensitic occurrences please see the descriptions of Lime Creek and Tishomingo.

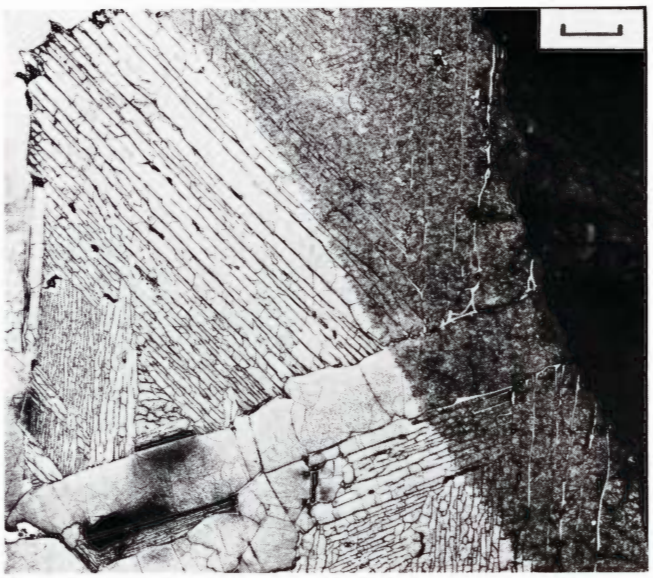

Figure 135. Thule (Copenhagen no. 1955, 186). Taper section through the heat-affected α_2 zone of a relatively well-preserved medium octahedrite. The slightly corroded surface is to the right. Etched. Scale bar 1 mm.

Massive transformation

The austenite of high purity Fe-Ni alloys (<0.01% C and < 7% Ni) will upon very rapid cooling (> 100° C per second) undergo a "massive transformation." The massive product is cubic α with irregular boundaries. The massive type of transformation occurs in many alloy systems and is intermediate in structural relationship, metallographic features and the amount of diffusion required between the normal nucleation and growth and martensite transformations (Massalski 1958; Swanson & Parr 1964; Speich & Swann 1965). For massive α to be formed in iron meteorites, the prerequisites seem to be very rapid cooling, almost carbon- and phosphorus-free nickel-iron and low nickel content. It would thus appear that massive transformation products are not present in meteorites.

Cohenite, $(Fe,Ni,Co)_3C$, is orthorombic and closely related to cementite, Fe_3C, which was described in steel at almost the same time (Howe 1890) as the identification of cohenite (Weinschenk 1889). Various works have later confirmed the crystallographical identity of cohenite and cementite and presented precise structural data (Westgran & Phragmen 1924; Illner 1969). From analyses quoted in the literature and from data by Scott (personal communication) it appears that cohenite contains 0.7-2.3% Ni and 0.02-0.3% Co. Reports that P should be present are erroneous and probably caused by the frequent small schreibersite inclusions.

Cohenite is brilliant white and strongly anisotropic. It is very hard, but also ductile, so that it will often support a Vickers diamond pyramid indentation without fracturing. Its hardness (50-100 g loads) is 1100±50, significantly higher than that of screibersite.

Figure 136. Canyon Diablo (Copenhagen no. 34.4045). Three cohenite crystals of the typical group I morphology. Where they meet, in upper left corner, brecciated schreibersite is present. The kamacite is shock-annealed to α_2. Etched. Scale bar 500 μ.

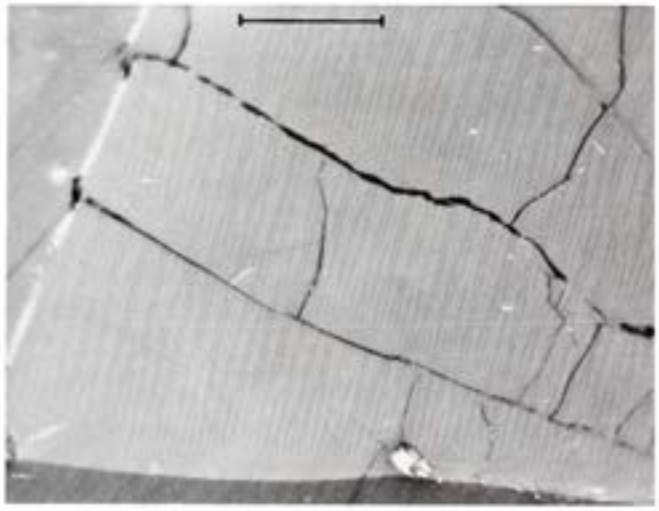

Figure 137. Toluca. Swathing cohenite around schreibersite (left). In the cohenite a stripe pattern of magnetic domains is seen. More complex patterns occur within other cohenite crystals of the same meteorite. Oil immersion. Crossed polars. Scale bar 100 μ. (Courtesy E. Scott.)

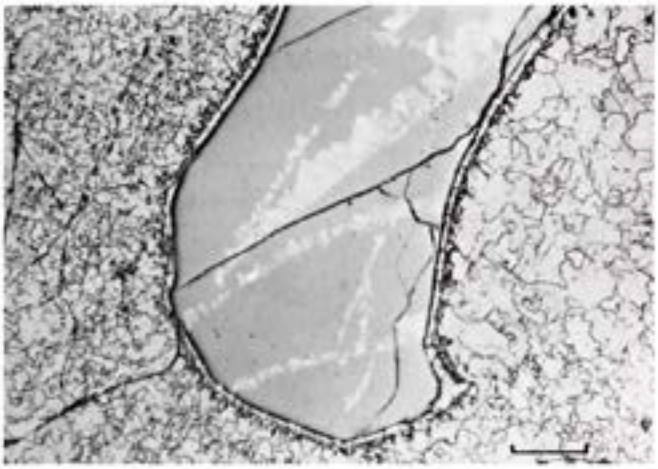

Figure 138. Canyon Diablo (Copenhagen no. 34.4045). Shock-annealed sample from the crater field. The large cohenite crystal has recrystallized along shear zones, and the rims are decomposed. The kamacite is of the shock-annealed α_2 variety. Etched. Scale bar 100 μ. Crossed polars.

A stripe pattern which becomes visible under crossed Nicols with strong illumination was shown by Heide (1966) to be a Bitter pattern of magnetic domains, revealed by the Kerr magneto-optical effect. See Figure 137.

Reheating, particularly of shocked iron meteorites (Canyon Diablo, Morasko), causes strained cohenite to recrystallize. Fractured cohenite will, upon prolonged reheating, ultimately decompose to ferrite and graphite. See, e.g., Hex River, Santa Rosa, Wichita County, Dungannon and Oscuro Mountains.

Cohenite is characteristic of group I but also occurs in many other iron meteorites. In column 13 of Appendix I, observed cohenite occurrences are indicated by Co.

Haxonite, (Fe, Ni, Co)$_{23}$C$_6$, is a new cubic mineral which was identified by Scott (1971) from X-ray powder photographs of Toluca material. It is structurally similar to $M_{23}C_6$

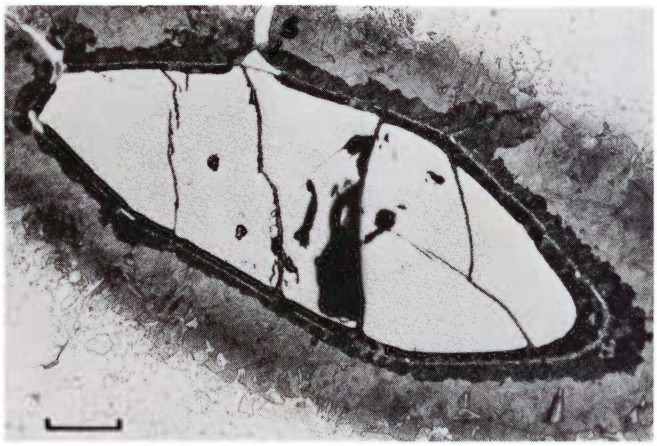

Figure 139. Odessa (Copenhagen no. 1961, 557). Reheated for 10 minutes to 850° C in the laboratory. The cohenite crystal has decomposed along fissures and along the interface with kamacite. Decomposition is prevented where schreibersite (S) opposes carbon diffusion. Etched. Scale bar 100 μ.

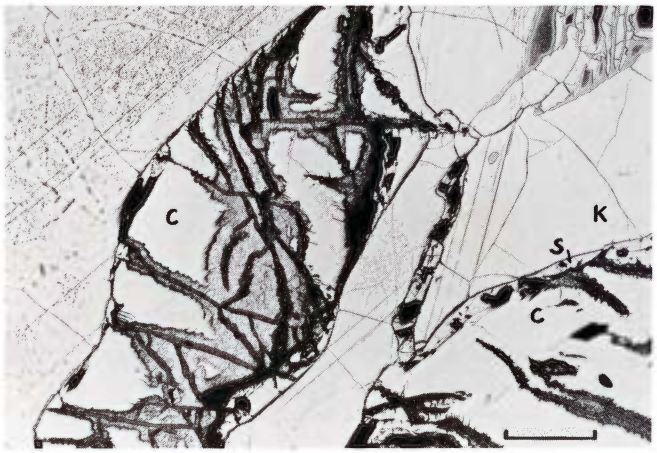

Figure 140. Wichita County (Copenhagen no. 1905, 1743). Cohenite crystals (C) under decomposition to columnar ferrite and lamellar graphite. Schreibersite (S), kamacite (K). Compare Figure 97. Etched. Scale bar 300 μ.

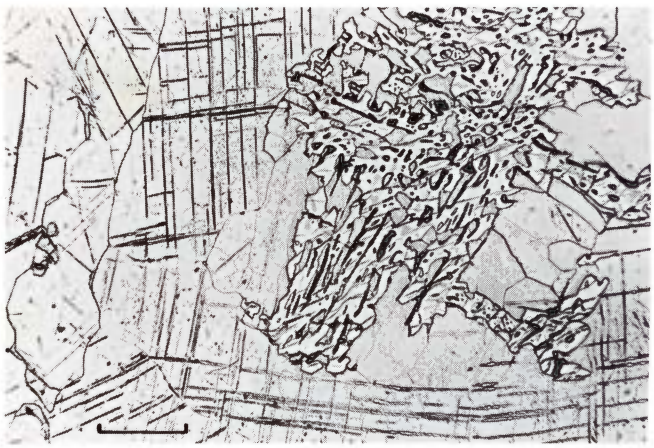

Figure 141. Santa Rosa (Tempe no. 103b). A palmate cohenite crystal with inclusions of taenite, kamacite and schreibersite. Recrystallized kamacite with Neumann bands. Etched. Scale bar 200 μ.

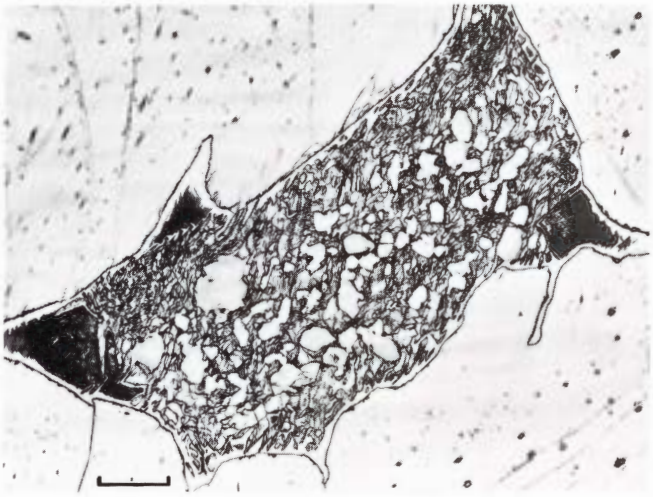

Figure 142. Mbosi (U.S.N.M. no. 2599). Differently oriented cohenite crystals within the same plessite field. Cold-worked, possibly due to artificial chiseling. Etched. Scale bar 100 μ.

carbides in steel, e.g., $Cr_{23}C_6$, but is itself unknown in steels. Haxonite shows a Ni range of 3.5-5.6% (and a Co range of 0.05-0.4% according to Scott). This is in harmony with the haxonite occurring in the more nickel-rich plessitic parts of the iron meteorites, and, chemically, it makes it distinctly different from cohenite. The author had, in fact, noted and measured the new mineral in Coopertown, Rhine Villa and Mungindi when its final identification was published by Scott.

Haxonite is brilliant white and hard. It is distinguished from cohenite by its isotropic behavior in reflected light and its somewhat lower hardness, 850±50. It rarely forms large massive crystals, but usually occurs as "carbide-roses" i.e., intricate intergrowths with taenite, schreibersite and kamacite particles. Haxonite is a minor accessory which frequently occurs in the same meteorites as cohenite. It appears to be characteristic of group I and group IIIC-IIID and is also present in nickel-rich meteorites, such as San

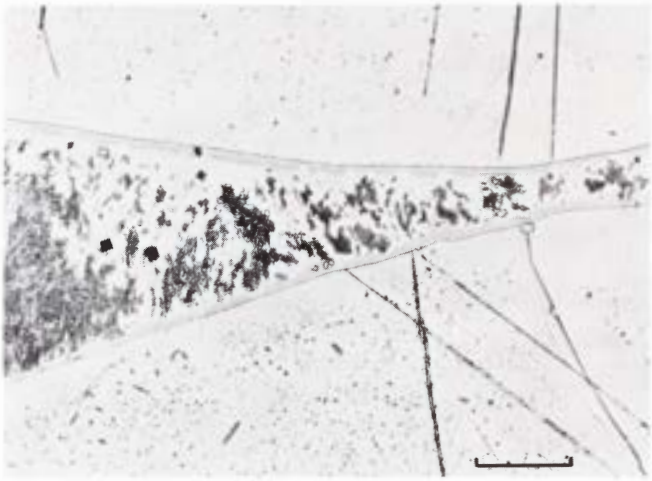

Figure 143. Shrewsbury (Copenhagen no. 1910, 301). Typical pearlitic plessite field with haxonite (brilliant white). The two Vickers hardness impressions at left indicate a hardness of 850 and significant ductility. Etched. Scale bar 100 μ.

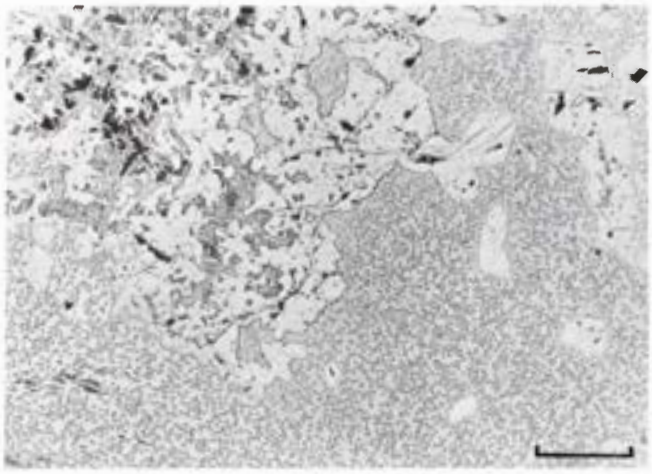

Figure 144A. Mungindi (U.S.N.M. no. 2944). Haxonite precipitated within spheroidized plessite and enveloping numerous tiny taenite, kamacite and schreibersite particles. Compare Figure 144B. Etched. Scale bar 200 μ.

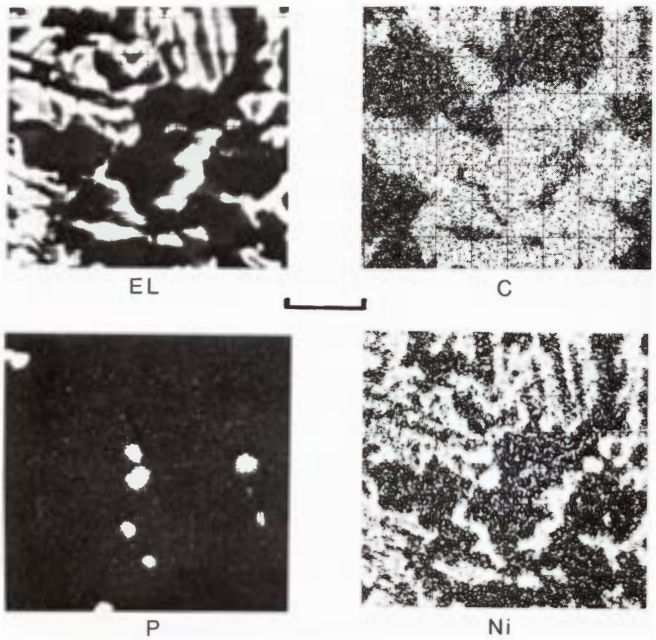

Figure 144B. Mungindi (U.S.N.M. no. 2944). X-ray scanning pictures of area from Figure 144A. The carbon radiation indicates the location of haxonite, the phosphorus radiation of schreibersite, and the nickel radiation that of taenite (and schreibersite). Scale bar 50 μ.

Cristobal and Lime Creek. Observed occurrences are indicated by an H in column 13 of Appendix I.

While carbides are virtually absent in the mainstream of group IIIA-IIIB – very minor cohenite particles occur in some low-Ni IIIA members, – there are a few irons with 7.9-8.8% Ni that contain haxonite or its graphitic decomposition products: Kokstad & Matatiele, Coopertown, Rhine Villa, Tanakami Mountains, Staunton, Paneth's Iron and Willow Creek. In other ways, too, these meteorites display structures slightly different from normal IIIA-IIIB irons, e.g., by having bulky and short kamacite lamellae. See Figure 146. Using Wasson's gallium data it may be seen on a

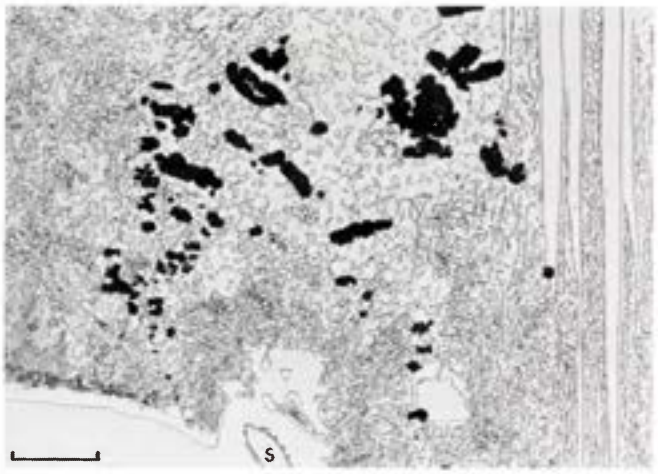

Figure 145. Willow Creek (U.S.N.M. no. 900). A spheroidized plessite field with graphite. The graphite is, in this case, almost certainly a decomposition product of haxonite. Note tiny taenite particles around the schreibersite crystal (S). Etched. Scale bar 40 μ.

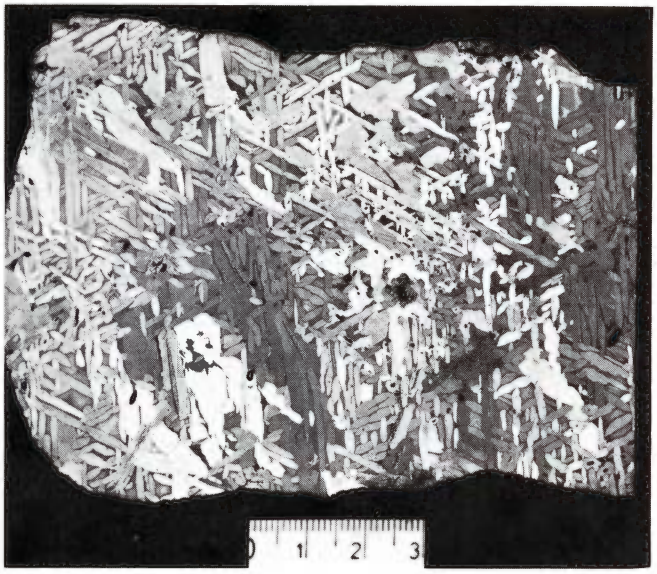

Figure 146. Willow Creek (U.S.N.M. no. 900). Even the macrostructure of this medium-coarse octahedrite is slightly anomalous compared to the mainstream of group IIIA-IIIB. It forms together with six other irons group IIIE. Etched. Scale bar in centimeters.

Ga-Ni plot (not shown) that the seven meteorites fall well below the IIIA-IIIB mainstream and thus form a separate group, IIIE (Scott et al. 1973). This is just another example of how accurate structural observations and chemical analyses support each other in the classification schemes.

Cohenite and haxonite – and cementite – are thermodynamically unstable at all temperatures at one atmosphere, ultimately decomposing to ferrite and graphite. What is surprising is that they survive at all in iron meteorites since these are considered to have cooled slowly and to have reached thermodynamic equilibrium. The present survey shows that the iron meteorites provide all stages, from undecomposed carbides (e.g., Cedartown, Wichita County) to fully decomposed (e.g., Hex River, Dungannon, Willow Creek). However, undecomposed carbides are more common than decomposed ones. It is suggested that the surprising stability is mainly due to the difficulty of nucleating graphite. Once nucleated along an internal crack or a cracked phase boundary, the graphite grows slowly at the expense of the carbides.

Carlsbergite, CrN is a new cubic mineral which was independently detected and identified by Scott and the author (Buchwald & Scott 1971). Particles extracted from heavily etched surfaces of Cape York were analyzed under the electron microprobe and afterwards studied by electron diffraction. It has a unit cell similar to synthetic CrN found in some steels.

Carlsbergite occurs as minute oriented laths, typically 30 X 5 X 2 in size, in the kamacite and as irregular 3-10 μ grains in some grain boundaries, Figures 148, 149A-B. Although small, carlsbergite attains significantly larger dimensions than the corresponding precipitates in steel that

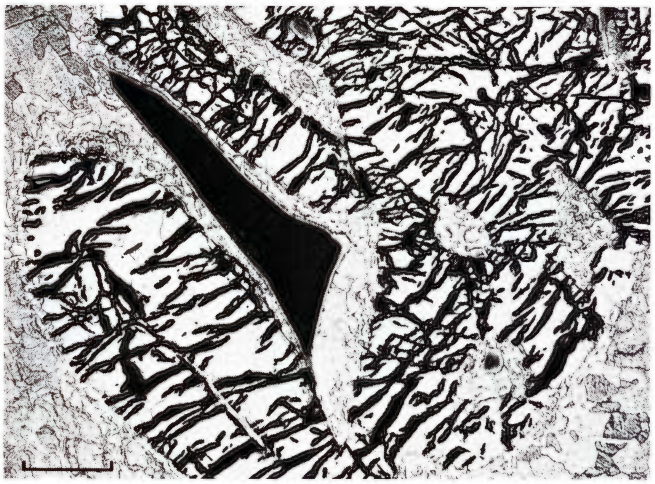

Figure 147. Dungannon (U.S.N.M. no. 644). The magnificent appearance of this section is caused by the complete decomposition (in space) of cohenite to graphite lamellae and recrystallized kamacite. A wedge-shaped black taenite field is also seen. Etched. Scale bar 400 μ. (Perry 1944: plate 62.)

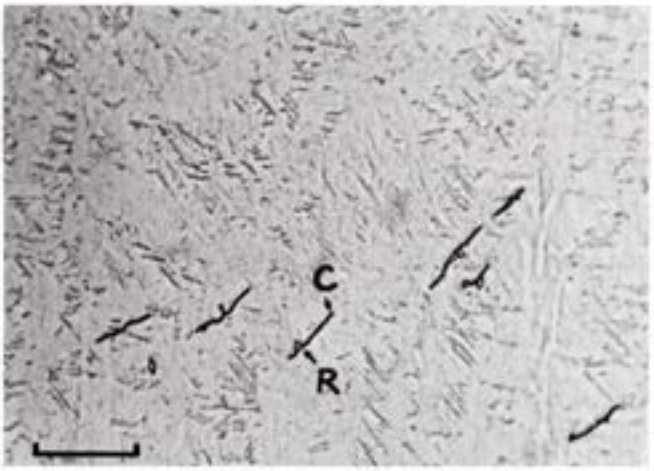

Figure 148. Russel Gulch (Tempe no. 307.1). Distorted carlsbergite platelets (C) in a shock-deformed kamacite matrix. The carlsbergite is often associated with tiny rhabdite particles (R). Etched. Scale bar 20 μ.

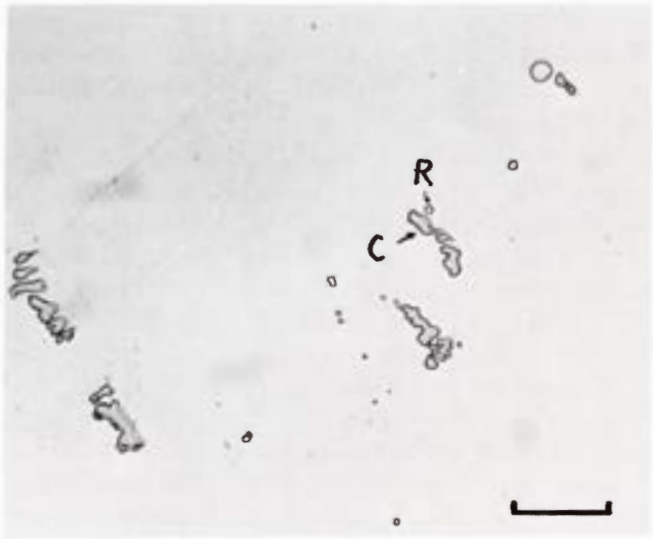

Figure 149A. Roebourne (U.S.N.M. no. 459A). Carlsbergite particles. This particular meteorite is cosmically annealed. The annealing caused the carlsbergite to separate from the associated rhabdite particles and to spheroidize slightly. Polished. Scale bar 10 μ.

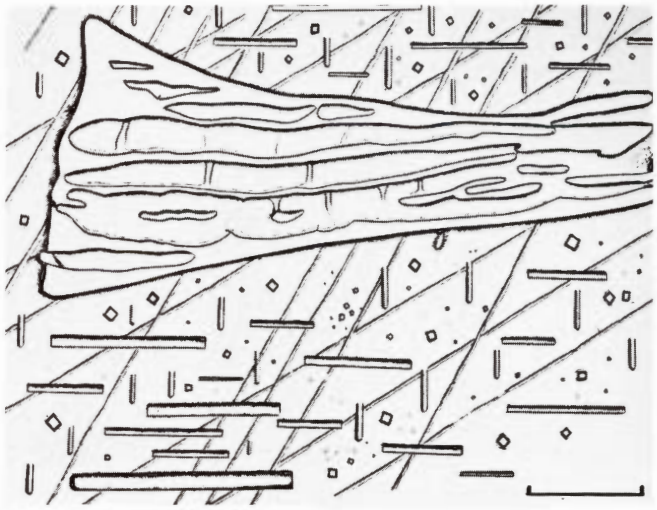

Figure 150. Seeläsgen. One of Rose's original drawings when he first described rhabdite (1864: plate 1). He was probably the first to examine gelatine imprints removed from an etched surface and placed under the microscope. It is remarkable how many details he could observe. Scale bar 100 μ.

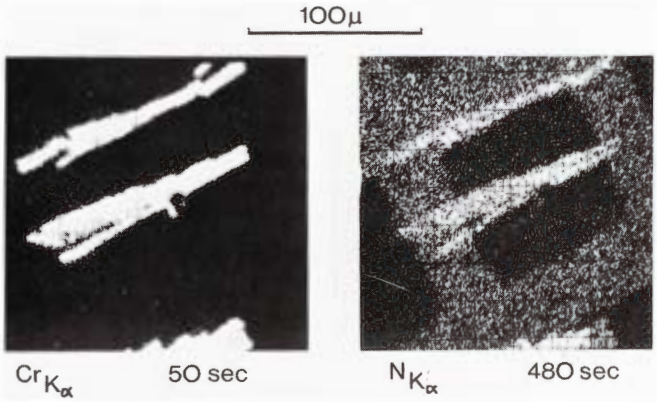

Figure 149B. Cape York (Copenhagen no. 1967, 410). X-ray scanning pictures of carlsbergite platelets extracted from the Agpalilik specimen. Taken with CrK_α and NK_α radiation. Continuous radiation from the supporting copper grid is visible only because of the much poorer peak to background conditions under which the right photograph was taken. (Buchwald & Scott 1971.)

Figure 151. Cape York (Agpalilik) (Copenhagen no. 1967, 410). Typical grain boundary precipitate of schreibersite. Because of its brittle nature, it is rich in microfissures, caused by cosmic deformations. Upon routine polishing the segments are unfortunately easily torn out, with the double effect of leaving black holes and deep scratches across the metallic components. Etched. Scale bar 100 μ.

require electron microscopy for their observation.

Carlsbergite is best observed on polished, unetched sections where – because of high hardness – it stands in high relief. It is isotropic and light gray with a distinct rose tint. It is a minor accessory, but quite common, particularly in the low-nickel end of group IIIA, where the carlsbergite platelets may occur with a frequency of 25 per mm^2.

Schreibersite and Rhabdite, $(Fe,Ni)_3P$. Schreibersite was originally described, somewhat inadequately, by Haidinger (1847). Later Rose (1864a) discovered rhabdite, correctly identifying it with schreibersite and observing the peculiar prismatic habit of the rhabdites. Particularly important studies have been published by Cohen (1894: 118), Wherry (1917), Böggild (1927), and Perry (1944). The studies by Goldstein & Ogilvie (1963), Reed (1965a; 1969), Buchwald (1966), Comerford (1969b) and Doan & Goldstein (1970) have added to accurate analyses for a number of occurrences and for the ternary Fe-Ni-P diagram.

Schreibersite is magnetic; it is tetragonal and yellow in reflected light. Compared to cohenite it is distinctly more brownish; it is also softer (H 800-950) and definitely more brittle – enough so that a Vickers diamond pyramid indentation usually shatters the mineral if it has not already been shattered as a result of cosmic event.

The composition is variable; generally the large skeleton crystals, which were precipitated early and directly from taenite, have low Ni-contents (~ 10-15%) and are hard (900-950) and brittle. The later crystals, which are of vermicular shape and located in the α - α and α - γ grain

boundaries and inside plessite, display higher Ni-contents (~ 20-50%) and are slightly softer (800-900) and more ductile. The rhabdites, which are 1-25 μ thick tetragonal prisms precipitated in the interior of the kamacite, also have high Ni-contents (27-50%) and are relatively soft (800-900) and ductile. They display few or no internal cracks.

When the phosphides happen to be located in the heat-affected α_2 rim zone, they may serve as built-in thermometers for registration of the steep temperature gradients developed during the atmospheric flight (Buchwald 1961b; 1967b). They will melt when rapidly reheated above 1100° C. If doubt arises as to whether a specific mineral is a carbide, schreibersite or something else, the mineral should be looked for in the heat-affected zone. Here, the phosphides just melt, creating rounded cavities, while the carbides partially melt and/or partially decompose, sending carbon out in solid solution (→ bainite) and precipitating minute graphite particles.

Schreibersite is present in numerous meteorites but not in all. It is absent in the low–Ni end of group IVA (e.g., Gibeon) and in, e.g., Arlington, Ysleta and Santiago Papasquiaro. When the bulk analytical value in group IVA increases above 0.06% P, the first minute schreibersite particles become visible. In group IIIA, a bulk value of more than 0.25% P causes large angular schreibersite crystals to precipitate directly from the taenite phase on cooling. When phosphorus is abundant (i.e., above ~ 0.4% P), the angular plate-like crystals may be seen to be oriented in dodecahedral directions, $\{110\}_\gamma$, of the parent taenite. They are then called Brezina lamellae (Cohen 1905: 252; Spencer 1951).

The widths of the schreibersite halos around troilite are proportional to the bulk P-value of the meteorite and inversely proportional to its cooling rate. The halos are early solid state precipitates which in their turn served as

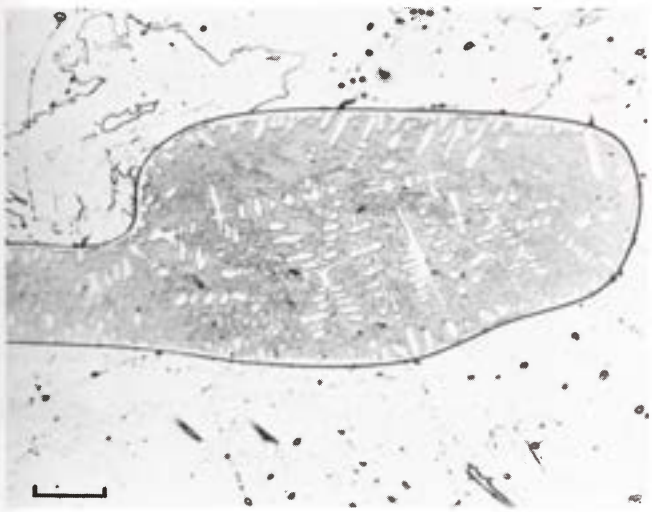

Figure 152. Silver Crown (U.S.N.M. no. 522). A completely molten and rapidly solidified schreibersite inclusion situated in the heat-affected A zone. Compare Figures 45 and 50. Etched. Scale bar 50 μ.

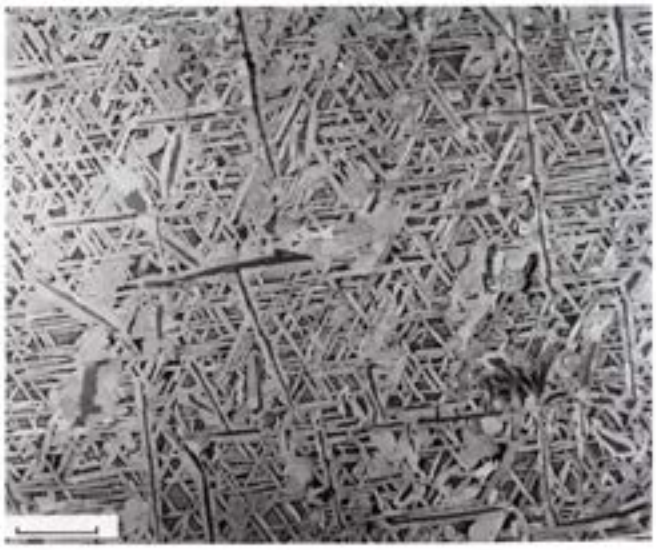

Figure 153. Grant (U.S.N.M. no. 836). A medium octahedrite of group IIIB with numerous oriented schreibersite lamellae, each of which displays rims of swathing kamacite. Although not analyzed in this case, the lamellae are apparently typical Brezina lamellae. Etched. Scale bar 10 mm. S.I. neg. M-127B.

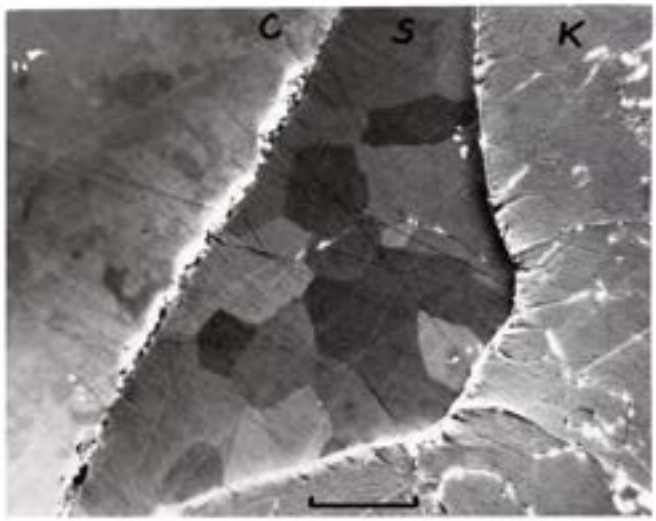

Figure 154. Canyon Diablo (Copenhagen no. 18463). In rare cases, as in this shock-annealed Canyon Diablo specimen of stage VI (See page 391), the schreibersite (S) has recrystallized. K is kamacite, C cohenite. In almost all other cases, schreibersite and rhabdite occur as monocrystalline units. Etched. Crossed polars. Scale bar 40 μ.

nuclei for rims of cohenite (in group 1) and kamacite (in all groups).

Rhabdites are prismatic or plate-shaped (Böggild 1927; Heide et al. 1932; Doenitz 1968) and occur abundantly in hexahedrites. Subgroups of hexahedrites with clearly defined ratios of prismatic to plate-shaped rhabdites may be distinguished. The prismatic rhabdites occur abundantly in many octahedrites (IIB, I, IIIA-IIIB). They are well developed in group I, e.g., in Canyon Diablo and Bischtübe; in some IIIB irons, e.g., Smith's Mountain, the rhabdites attain the unusual thickness of 50 μ.

Barringerite. Barringerite, $(Fe, Ni)_2P$, was recently reported by Buseck (1969). The present author believes that

Figure 155. Uwet (U.S.N.M. no. 601). Plate-shaped rhabdites in a hexahedrite. Below, a cohenite crystal that has decomposed to graphite (black) and ferrite. Etched. Scale bar 500 μ.

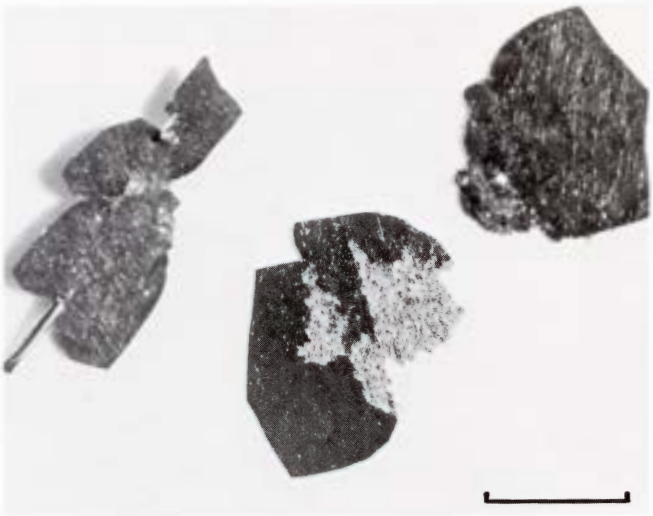

Figure 156. Richland (U.S.N.M. no. 1735). Plate-shaped rhabdites, isolated by dissolving the metallic matrix in acid. The surfaces are brilliant black and striated, probably due to shear-deformation by cosmic shock. Scale bar 2 mm. (From Henderson & Monnig, 1956.)

Figure 157. Youndegin (U.S.N.M. no. 3157). Prismatic rhabdites in a coarse octahedrite. Here, the slender tetragonal prisms are sectioned in 5 different orientations. A grain boundary with minute phosphide precipitates is also visible. Slightly etched. Scale bar 50 μ.

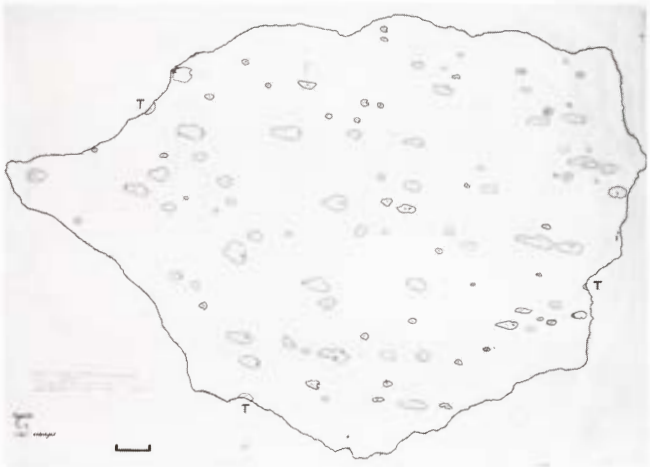

Figure 158. Cape York (Copenhagen). An accurate sketch of the morphology of the oriented troilite crystals, revealed on the 180 x 125 cm large endpiece, cut from the 20-ton Agpalilik mass. In three places (T) the troilite is partially ablated away in the atmosphere. Scale bar 10 cm. Compare Figures 189C and 510.

the mineral is not of cosmic origin but a secondary product, caused by the artificial reheating of a weathered meteorite (the pallasite Ollague). While the mineral is really there, it should be pointed out that it is one of those curious occurrences which owe their creation to human activity and has little significance when discussing the genesis of meteorites.

Troilite, FeS. The Jesuit father, Domenico Troili observed iron sulfide inclusions in the stone meteorite Albareto as early as 1766. Not until 100 years later could accurate analyses finally prove the sulfide to be different from pyrite, FeS_2 and pyrrhotite, $Fe_{1-x}S$. Haidinger (1863a) proposed the name troilite for the stoichiometric FeS. Reviews and excellent descriptions have been provided by Rammelsberg (1864), Cohen (1894: 182), Sims (1959), El Goresy (1965), and Perry (1944). On one point, however, Perry erred. On Plate 48 he correctly stated that troilite is hexagonal but his often quoted photomicrograph of Otumpa (i.e., Campo del Cielo) did *not* show a hexagonal troilite crystal but a section through a cliftonitic graphite crystal. The present author has, in fact, never observed, in iron meteorites, a troilite crystal with hexagonal facets toward the metallic matrix.

Pure troilite contains little other than FeS; the total amount of other elements (Ni, Co, Cu, Cr, Mn, Zn, Pb) may be estimated to be less than 1%. However, when exposed to shock compression and associated reheating, the troilite easily melts and then disperses and partially dissolves the encasing walls of schreibersite, cohenite or nickel-iron; also any daubreelite, silicate or chromite will be fractured and included. Thus, as noted by Nichiporuk & Chodos (1959), the troilite may be extremely heterogeneous.

Figure 159. Grant (U.S.N.M. no. 836). Troilite nodule with metal inclusion. Well-developed swathing kamacite. Brezina lamellae of schreibersite. Compare Figure 153. Etched. Scale bar 4 mm. S.I. neg. M-128A.

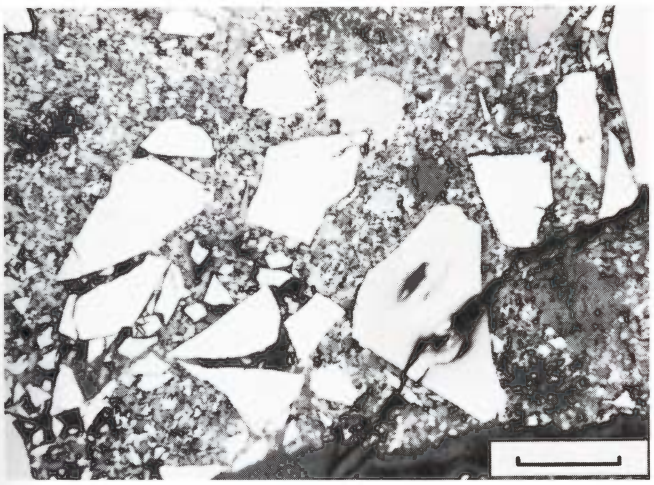

Figure 160. Pan de Azucar (the Carrizalillo specimen in Oslo). Shock-altered troilite. The troilite has been briefly melted and the associated schreibersite (white) has become shattered and dispersed through the melt. This solidified in a fine-grained eutectic. Polished. Crossed polars. Scale bar 40 μ.

Troilite is unmagnetic (if pure), bronze-colored with a greenish tint and strongly anisotropic. Its microhardness is 250±30 Vickers. It often includes parallel daubreelite lamellae and in group I, graphite, chromite and numerous silicates. Also, chromite and phosphate crystals are present in many group III troilite nodules.

Troilite melts at 1190° C and the Fe-S equilibrium diagram has a eutectic at 988° C (Hansen & Anderko 1958). Troilite is, therefore, easily ablated away in the atmosphere unless it contains a certain number of refractory inclusions such as graphite and silicates (See, e.g., Bogou). Troilite usually occurs as shapeless nodules, bars and dumbbells. The smaller ones may be bar-, diamond- or plate-shaped. The parallel orientation of large troilite nodules, reported from Cape York and Santa Rosa (Buchwald & Wasson 1968; Buchwald 1971c) may be more universal than hitherto believed.

At austenitic temperatures troilite, chromite and taenite were the only phases present in many iron meteorites. Therefore, when the taenite cooled and started to

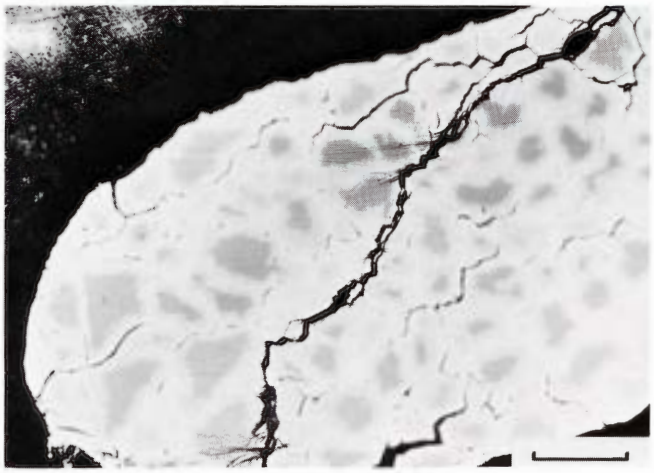

Figure 161. Twin City (U.S.N.M. no. 1770). Recrystallized troilite inclusion that has subsequently been altered by terrestrial corrosion. One of the alteration products (white) is pentlandite, $(Fe,Ni)_9S_8$. Etched. Scale bar 20 μ.

decompose, the first kamacite and schreibersite to precipitate formed heterogeneously upon the available troilite and chromite nuclei. That is why so many troilite and chromite inclusions are wrapped in successive sheets of various minerals. Beautiful examples are to be found in, e.g., Canyon Diablo, Coahuila, Sikhote-Alin, Cape York, Chupaderos and Wiley.

Reichenbach lamellae were seen by Reichenbach (1861, etc.) and named by Brezina (1880b). When best developed, they form very thin (< 0.05 mm), but large (20 × 30 mm) platelets in three directions parallel to $\{100\}_\gamma$. Additional directions are often present, e.g., in Cape York. Unfortunately, the lamellae are difficult to examine because they are thin and often broken and easily

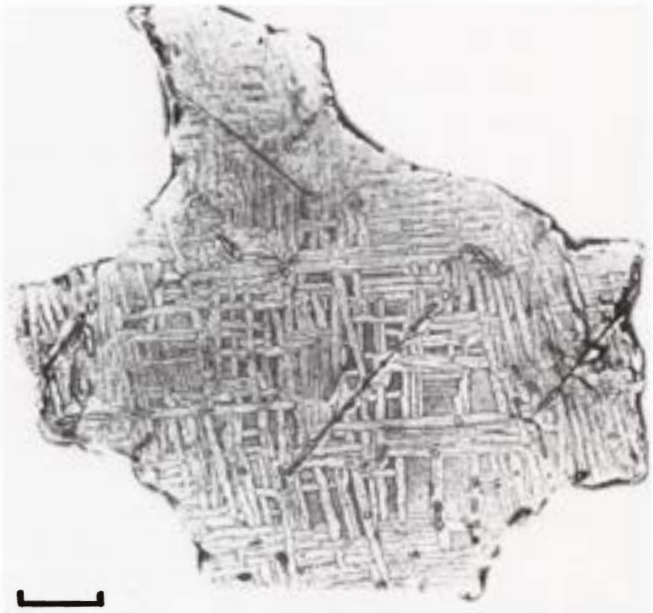

Figure 162A. Ilimaes (Vienna). The first figures of Reichenbach lamellae were provided by Tschermak, who deep-etched sections of the medium octahedrite Illimaes. Scale bar 10 mm. (From Tschermak 1872b).

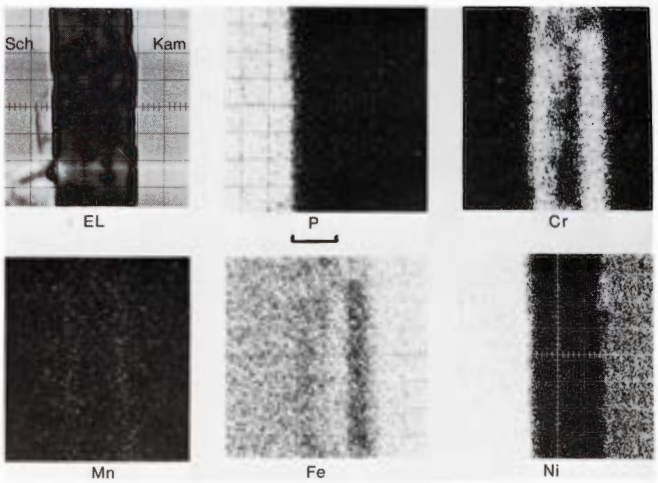

Figure 162B. Cape York (Agpalilik) (Copenhagen no. 1967, 410). In the center, a typical Reichenbach lamella of chromite. To the right, kamacite; to the left, schreibersite nucleated by the chromite. Significant rims of nucleated troilite are also present but not shown here. X-ray scanning pictures taken with electrons (EL) and with PK_α, etc., radiation, as indicated. Scale bar 10 μ.

corroded. Usually when the present author has had a well-preserved Reichenbach lamella under the microscope and under the microprobe, it surprisingly turned out that the lamellae were not, as hitherto believed, pure troilite lamellae but were composed rather of primary, ultrathin (1-5 μ) chromite lamellae upon which secondary troilite had later nucleated. In other words, the chromite must have determined the crystallographic relationships with the taenite and the formation must have taken place at a considerably higher temperature and because of a different mechanism than that proposed by Brett & Henderson (1967). It can, however, not be ruled out that some Reichenbach lamellae consist only of thin troilite sheets and can have formed as crack-fillings (Brett & Henderson 1967).

Troilite is virtually omnipresent in iron meteorites. It is probably absent in Nedagolla and Tucson. Because it is so

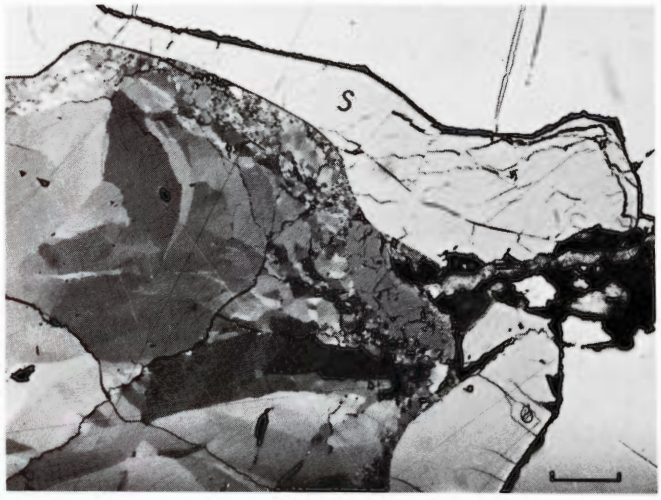

Figure 163. Waterville (Tempe no. 453.2x) Troilite with undulatory extinction (left) and recrystallized portions adjacent to the brecciated schreibersite (S). Etched. Scale bar 50 μ.

sensitive to shock events it will probably be – together with kamacite and taenite – eminently suited to reveal the cosmic shock and annealing events. In column 12, Appendix I, the presence of troilite is indicated; X: present, but not examined in a polished section. 1: Monocrystalline. 2: Deformed, displaying multiple twinning. 3: Deformed, with undulatory extinction. 4: Recrystallized. 5: Shock-melted and transformed to fine-grained eutectics.

Graphite, Diamond and *Lonsdaleite*. Graphite, C. The first substantiated report of graphite in iron meteorites was by Troost (1840). Numerous observations have been added later, e.g., by Reichenbach (1862b), Smith (1876a), Cohen (1894: 148), Perry (1944), El Goresy (1965), Marshall & Keil (1965) and Buchwald & Wasson (1968).

Graphite occurs as centimeter-sized nodules in association with troilite and silicates in group I and I-Anomalous. Outside these groups, graphite-troilite nodules are rare or absent. Fine graphite lamellae and spherulites, that usually are the decomposition products of former carbides, occur in group IIA, IID, IIID, IIIE and several anomalous irons. Butler, e.g., shows intriguing spherules with serrated edges which can be observed with the naked eye on polished sections. They resemble shock-affected troilite nodules and may have a similar origin.

Cliftonitic graphite – i.e., graphite crystals that, in sections, display cubic, cubo-octahedral and pseudo-hexagonal outlines (Figure 166) had been observed by Haidinger (1846) and was named cliftonite by Fletcher (1887c). (See page 792, Magura.) The cliftonite is apparently not a pseudomorph after diamond but rather a solid state precipitate of C in kamacite, in which the external faces of the growing graphite are governed by the cubic structure of kamacite and thus assume cubic outlines.

Brett & Higgins (1967) demonstrated that graphite aggregates of cubic morphology could, in fact, be grown in

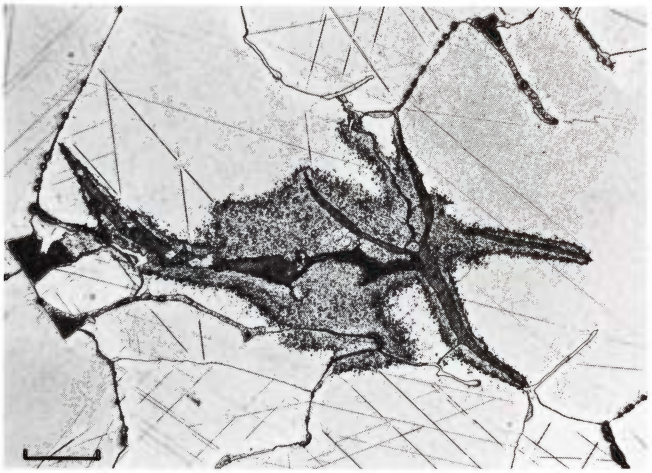

Figure 164. Willamette (U.S.N.M. no. 333). Severely altered troilite in recrystallized kamacite. Shock and subsequent annealing altered an original troilite lens to a fine-grained eutectic with spidery filaments of melted sulfides. Etched. Scale bar 50 μ.

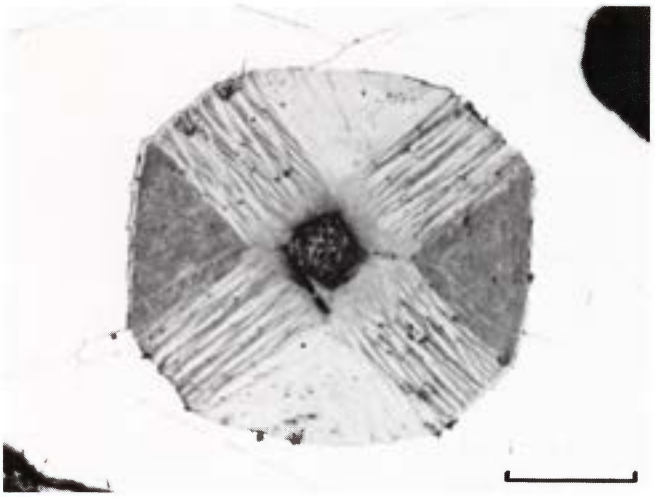

Figure 166. Seligman (U.S.N.M. no. 1761). Graphite occurs in the kamacite phase as cliftonitic units with fine, oriented extinction. Etched. Crossed polars. Scale bar 100 μ.

Figure 165. Odessa (Tempe no. D91.91). Typical graphite (G)-troilite (T) intergrowth with about equal parts of the components. So-called horsetail extinction. Polished. Crossed polars. Scale bar 20 μ.

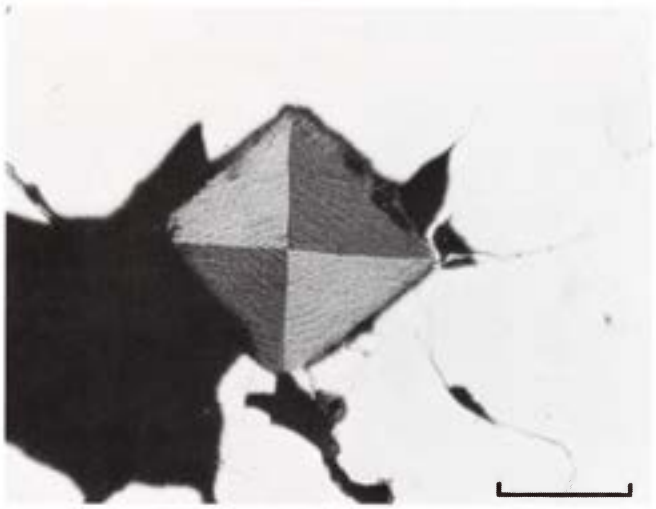

Figure 167. Seligman (U.S.N.M. no. 1761). The cliftonitic graphite may also assume square outlines. Etched. Crossed polars. Scale bar 100 μ.

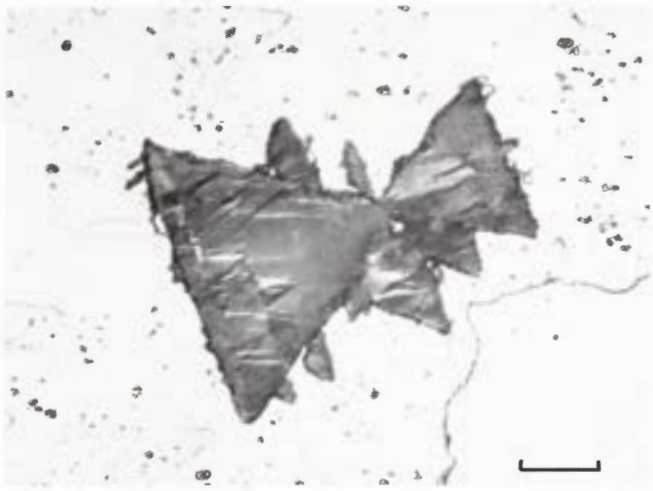

Figure 168. Kendall County (U.S.N.M. no. 1657). Triangular or arrowhead development of graphite occurs in a few meteorites, such as Kendall County, Morrill and Mundrabilla. The graphite precipitates are oriented with respect to the cubic kamacite lattice. Etched. Crossed polars. Scale bar 20 μ.

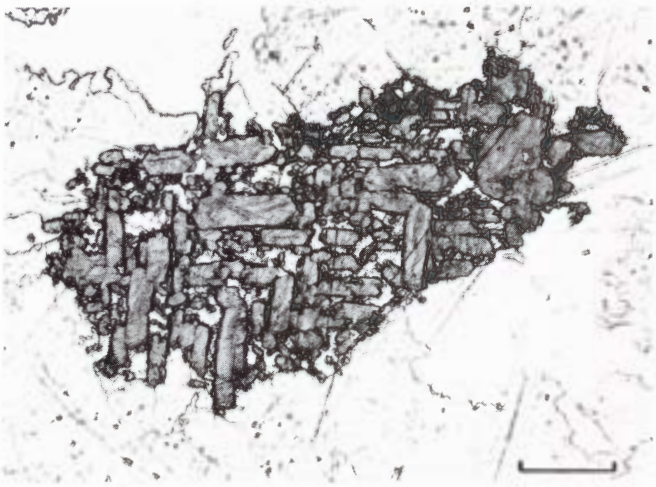

Figure 169. Kendall County (U.S.N.M. no. 1657). Basket weave precipitates of graphite in kamacite. This morphology seems to be restricted to a few anomalous iron meteorites. Etched. Scale bar 40 μ.

the laboratory by annealing Fe-Ni-C alloys for about 1000 hours at one atmosphere and 550° C.

In column 12, Appendix 1, a G indicates the presence of graphite, Gc the presence of cliftonitic graphite, and Cg the presence of a carbide under decomposition to graphite.

Diamond, C. Koenig stated in Foote's paper (1891) that small diamonds occurred in some Canyon Diablo specimens, and this has later been confirmed from many sides (Nininger 1939d; Ksanda & Henderson 1939; Moore et al. 1967). Since many of the heat-affected specimens contain diamonds, yet diamonds have not been found in any of the unaltered fragments, Nininger (1956) suggested that the temperatures indicated were those required to form diamonds from graphite during the passage of a shock wave front caused by the cratering impact of Canyon Diablo. Lipschutz & Anders (1961) and Heymann et al. (1966) supported this hypothesis, and the present author must also conclude that this is the most likely explanation for the diamond occurrences. See also Canyon Diablo page 384 and Magura page 793.

Lonsdaleite, C. Frondel & Marvin (1967) showed that many of the carbonados in Canyon Diablo, normally accepted as diamonds, were in fact aggregates of diamond and a hexagonal polymorph of diamond, which they named Lonsdaleite. Lonsdaleite was no doubt formed by the same shock waves that produced the diamonds. See page 385.

Daubreelite, $FeCr_2S_4$, was discovered by Smith (1876c) in the hexahedrite Coahuila, where it occurs abundantly, particularly in its typical variety: as parallel wide bars in troilite. Cohen (1894: 209), Perry (1944), and El Goresy (1965) added many observations, and Heide et al. (1932) and Lundquist (1943) determined the structure to be that of a cubic spinel type. The ternary Fe-Cr-S system has been examined by Kullerud and co-workers, who have also discussed the conditions for the formation of daubreelite.

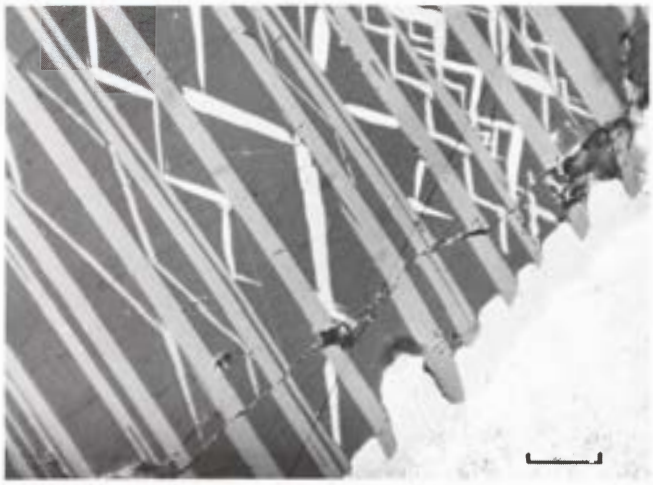

Figure 170. Iquique (Berlin). Daubreelite lamellae (gray) exsolved parallel to (0001) of the hexagonal troilite single crystal. Due to shock compression the troilite shows multiple twinning, with alternating white and black portions in crossed polars. Scale bar 20 μ.

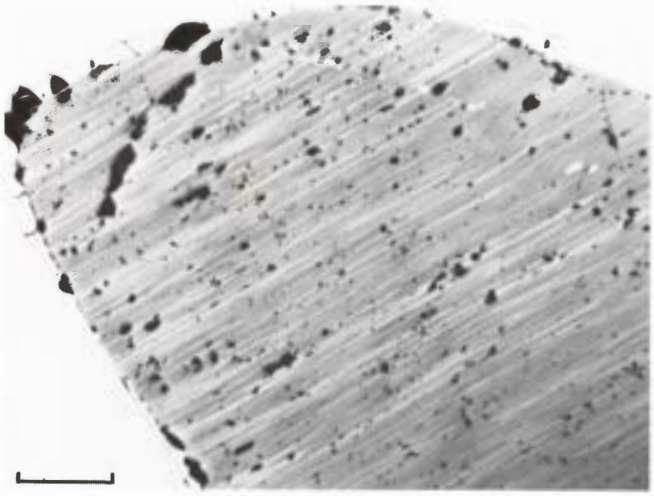

Figure 171. Walker County (U.S.N.M. no. 379). A sulfide nodule exhibiting alternating fine lamellae of daubreelite and troilite. A narrow, fissured rim of schreibersite and cohenite is also seen. Polished. Scale bar 100 μ.

The mineral is bluish and isotropic, with a Vickers hardness of about 400. It occurs as an exsolution product in troilite and here forms lamellae parallel to (0001) that range from 0.5 μ to 1 mm in widths. It appears that the ratio of daubreelite to troilite is inversely correlated with the size of the troilite nodule, the small nodules (0.1 mm) displaying up to 50% daubreelite. Daubreelite occurs particularly in group I, IIA, IIIA and IVA. Besides being present in troilite, it forms discrete 10-500 μ particles in kamacite.

Cosmic shocks and associated reheating usually entirely destroy the troilite-daubreelite aggregates. Thereby the daubreelite is shattered and partially dissolved, afterwards occurring as dispersed subangular particles, 1-10 μ in size, in the troilite.

Artificial reheating of troilite-daubreelite assemblages often causes the minerals to recrystallize; in the recrystallized grains very fine parallel exsolution lamellae form. See Figure 26. See also, e.g., Rodeo, Verkhne Udinsk and Yanhuitlan.

Chromite. Chromite, $FeCr_2O_4$, first mentioned by Shepard (1853b) and Rose (1864a), this mineral has later proved to be quite common in iron meteorites. Reviews have been published by Cohen (1894: 244) and scattered observations are to be found in various papers, e.g., by Derby (1895; 1896), Snetsinger et al. (1967) and Bunch & Keil (1971).

Chromite is a cubic spinel with prominent octahedral cleavage. It is bluish in reflected light and has a high Vickers hardness (> 1100), somewhat difficult to determine because it usually splits under the indentation load. It occurs as cubes and octahedra in troilite nodules of group I and IIIA and reaches large dimensions (8 × 4 cm) in Sikhote-Alin, Sacramento Mountains and in some pallasites, e.g., Brenham. As mentioned page 108, it forms the backbone of

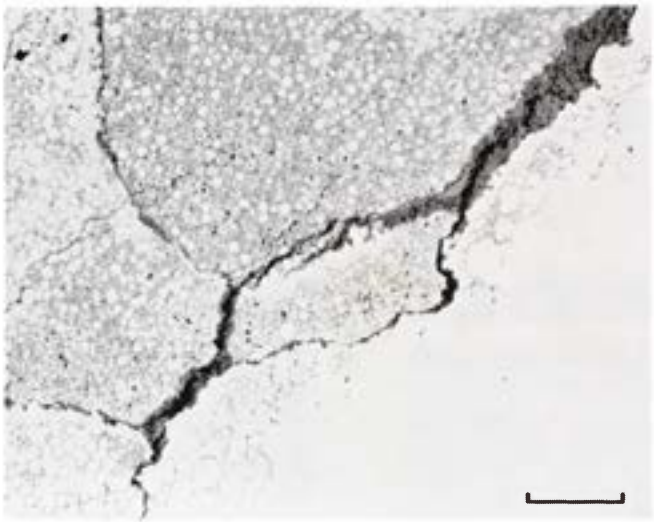

Figure 172. Dalton (U.S.N.M. no. 1010). In this medium octahedrite of group IIIA the original troilite-daubreelite nodules are entirely destroyed because of cosmic shock annealing. The iron sulfide forms a fine-grained eutectic with iron, while the daubreelite occurs as subangular 10 μ particles, dispersed through the melt. White is kamacite. Black is terrestrial corrosion. Polished. Scale bar 300 μ.

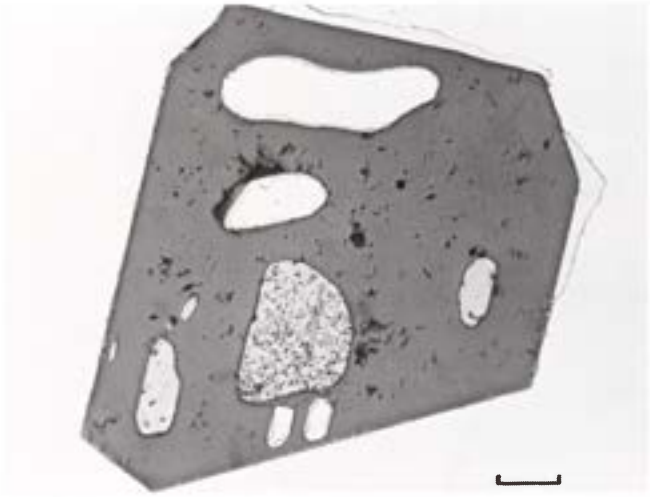

Figure 173. Zacatecas (1792) (Copenhagen no. 1906, 145). Cubic chromite crystal in kamacite. Four cavities are filled with kamacite. Narrow fringes of schreibersite are present along the interfaces. Also four inclusions of troilite (gray). Polished. Scale bar 50 μ.

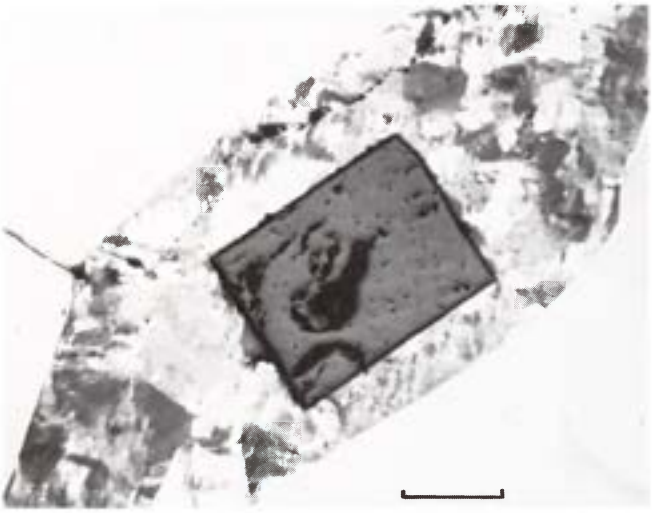

Figure 174. Cape York (Agpalilik) (Copenhagen no. 1967, 410). Cubic chromite crystal as a nucleus for a lenticular troilite crystal. Late deformation has damaged the troilite and subdivided it into numerous cells of different orientation. Polished. Crossed polars. Scale bar 300 μ.

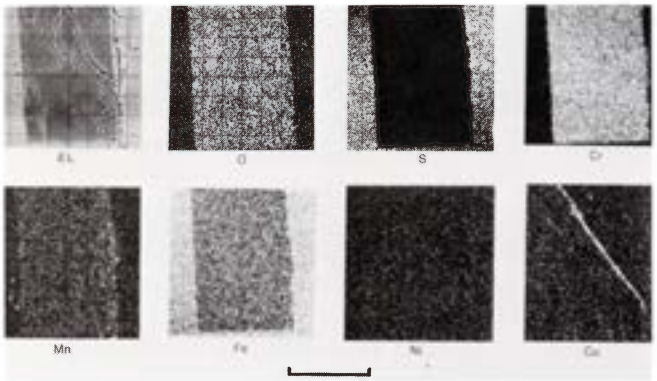

Figure 175. Cape York. X-ray scanning pictures of chromite in troilite, similar to Figure 174. It is seen that chromite is enriched in manganese, while Cu seems to be present as filaments of elementary copper in the chromite fissures. Scale bar 100 μ.

many Reichenbach lamellae, occurring as thin, but large, lamellae cutting through the Widmanstätten structure that developed after the chromite had precipitated from solid solution. Chromite is also present in many anomalous iron meteorites, e.g., N'Goureyma, Zacatecas and Monahans. See Figure 173.

Silicates. Silicate inclusions are present in a large number of iron meteorites (Bunch et al. 1970). The survey in Appendix I (silicates are in column 13 marked S) clearly shows that silicates are almost exclusively concentrated in group I and group I-Anomalous, having been detected in 36 of 88 meteorites of those categories. Further search will probably reveal silicates also in the remaining 52. In the 293 meteorites belonging to group IIA-IIB, IIC, IID, IIIA-IIIB, IIIC-IIID, IVA and IVB only six instances of very minor silicate inclusions were found. Finally, there were 17 instances of silicate-bearing meteorites among the 92 anomalous irons, Figures 177A-B.

Since the present study was mainly based upon polished sections and thus was not well adapted for the examination of non-opaque minerals, the silicates were

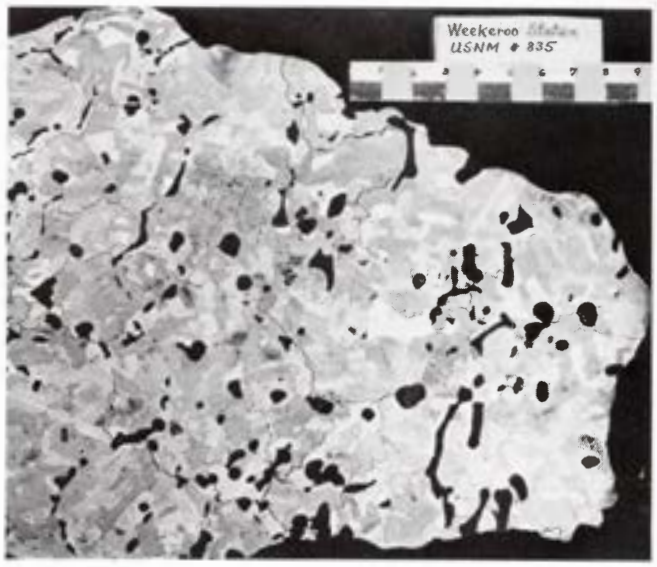

Figure 177A. Weekeroo Station (U.S.N.M. no. 835). Silicates in a polycrystalline iron meteorite. The silicates assume lamellar shapes in the original taenite grain boundaries but approach globular shapes in the grain interiors. Etched. Scale in centimeters.

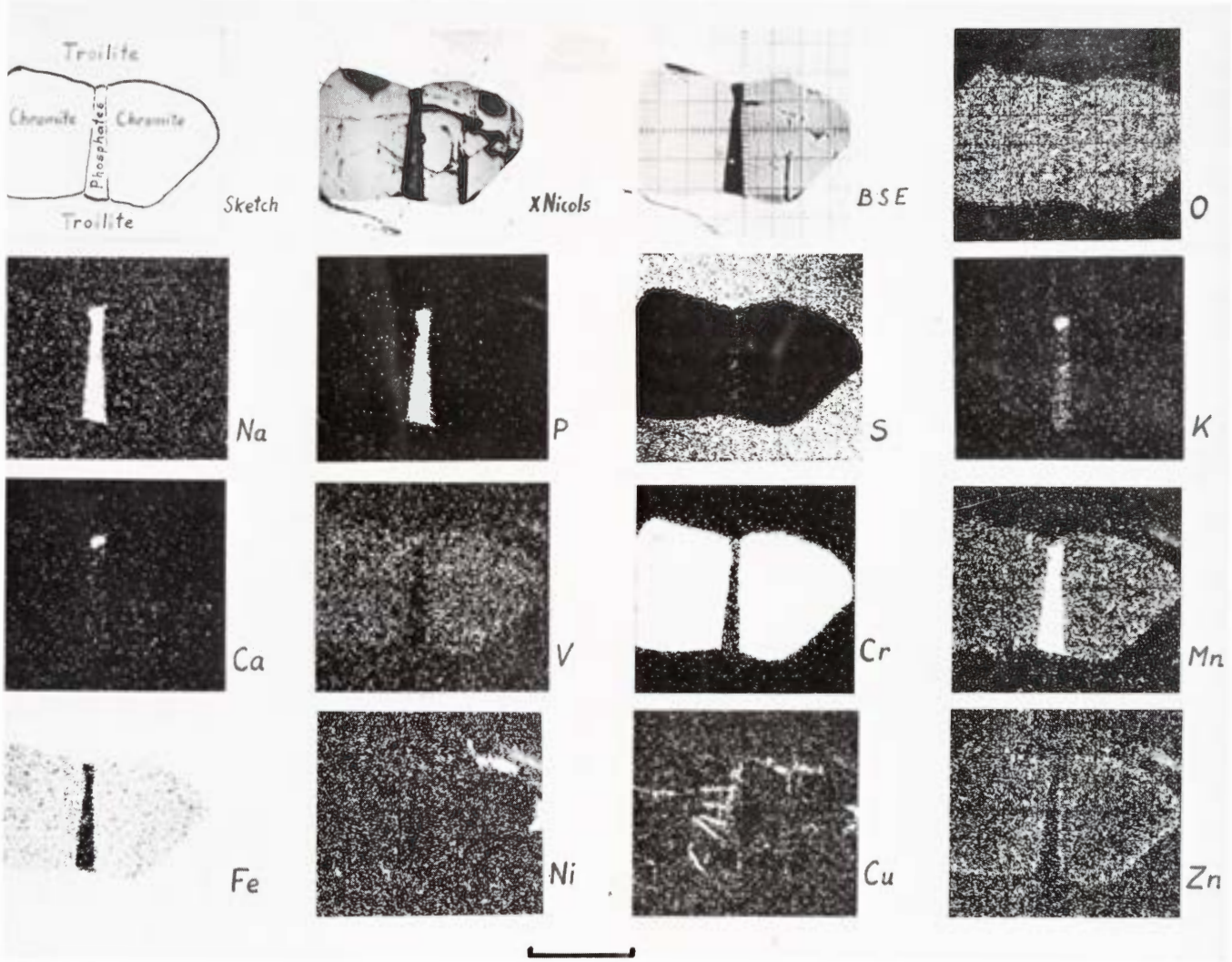

Figure 176. Cape York. X-ray scanning pictures of chromite and phosphates in a troilite nodule. The chromite is enriched in V, Mn, Zn (and Ti), and shows elementary copper in fissures. The phosphates are apparently (Mn, Na) PO_4 with accessory amounts of K and Ca. Scale bar 200 μ.

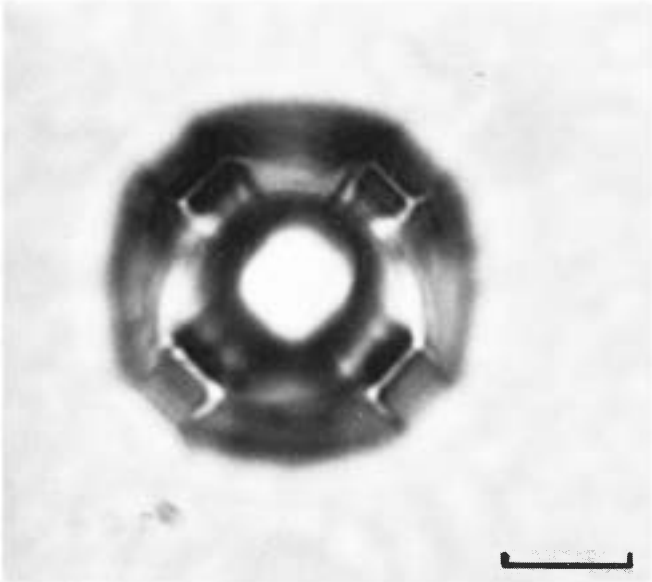

Figure 177B. Tucson (U.S.N.M. no. 368, Ring mass). A large number of the silicate inclusions in Tucson are small and equiaxial, and exhibit cubic crystal facets. Since the silicates themselves are monoclinic or orthorhombic, it appears that the cubic symmetry must have been imposed by the accomodation to the cubic taenite and kamacite phases. Polished. Oil immersion. Scale bar 10 μ.

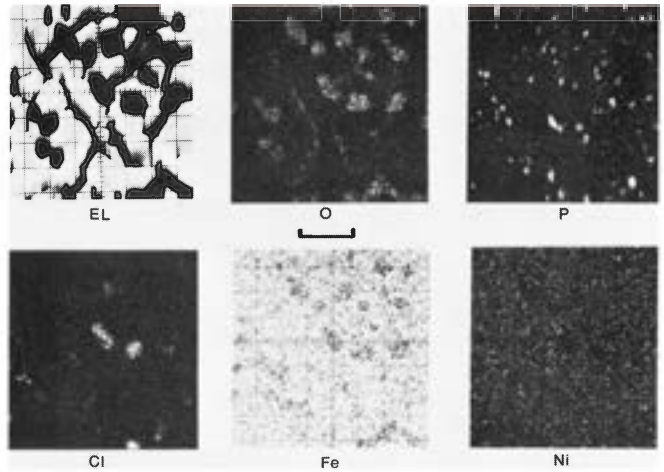

Figure 178. Wathena (U.S.N.M. no. 1387). A recrystallized and corroded hexahedrite. X-ray scanning pictures of near-surface areas indicate the presence of oxygen and chlorine. Chlorine is particularly concentrated in the zone of active weathering. Adjacent parts of the meteorite are entirely converted to chloride-free limonite and are now inactive. Scale bar 50 μ.

usually not determined further than to the broad categories, olivines, pyroxenes, plagioclases and glasses. However, the notes should enable any interested party to select the most promising material for study.

Doubtful Minerals

Moissanite, SiC, was reported by Moissan (1904), but has never again been observed. I agree with Merrill (1930) and Mason (1967a) that Moissan's material was contaminated with carborundum abrasive.

Lawrencite, $FeCl_2$, is a mineral which is supported by Cohen (1894: 227), Perry (1944: 25), Mason (1962a: 60) Keil (1969: 106) and Strunz (1970: 157). As discussed on page 82, the present author disagrees with the observations and concludes that virtually all chlorine observed in iron meteorites is of terrestrial origin. I assume that the mineral is totally absent in iron meteorites and probably does not exist at all. See also the discussion under Cranbourne, page 508.

Gold, Au. Edwards (1953) reported gold grains in Wedderburn, but it appears that the observation was based upon some misinterpretation. See page 1295.

Chalypite, Fe_2C, has been mentioned by Shepard (1867a) and Strunz (1970: 97). The identification is inadequate, and the mineral probably does not occur.

Gentnerite, $Cu_8Fe_3Cr_{11}S_{18}$, was described by El Goresy & Ottemann (1966) but apparently inadequately; it has been rejected by the International Mineralogical Association, and by Strunz (1970: 529).